



Michigan Technological University
Create the Future Digital Commons @ Michigan Tech

Dissertations, Master's Theses and Master's
Reports - Open

Dissertations, Master's Theses and Master's
Reports

2010

Theoretical estimation of optical absorption and photoluminescence in nanostructured silicon; an approach to improve efficiency in nanostructured solar cells

Jaspreet S. Nayyar
Michigan Technological University

Follow this and additional works at: <https://digitalcommons.mtu.edu/etds>


 Part of the [Electrical and Computer Engineering Commons](#)

Copyright 2010 Jaspreet S. Nayyar

Recommended Citation

Nayyar, Jaspreet S., "Theoretical estimation of optical absorption and photoluminescence in nanostructured silicon; an approach to improve efficiency in nanostructured solar cells", Master's Thesis, Michigan Technological University, 2010.
<https://doi.org/10.37099/mtu.dc.etds/50>

Follow this and additional works at: <https://digitalcommons.mtu.edu/etds>

 Part of the [Electrical and Computer Engineering Commons](#)

A THEORETICAL ESTIMATION OF OPTICAL ABSORPTION AND
PHOTOLUMINESCENCE IN NANOSTRUCTURED SILICON; AN APPROACH
TO IMPROVE EFFICIENCY IN NANOSTRUCTURED SOLAR CELLS

By

JASPREET S NAYYAR

A THESIS

Submitted in partial fulfillment of the requirements

for the degree of

MASTER OF SCIENCE IN ELECTRICAL ENGINEERING

MICHIGAN TECHNOLOGICAL UNIVERSITY

2010

© 2010 Jaspreet S Nayyar

This thesis, "A Theoretical Estimation of Optical Absorption and Photoluminescence in Nanostructured Silicon; An approach to Improve Efficiency in Nanostructured Solar Cells", is hereby approved in partial fulfillment of the requirements for the degree of MASTER OF SCIENCE in Electrical Engineering.

DEPARTMENT:
Electrical and Computer Engineering

Signatures:

Thesis Advisor _____
Dr. Anand K. Kulkarni

Department Chair _____
Dr. Daniel R. Fuhrmann

Date _____

This thesis is dedicated to my mom and dad, for their relentless affection and love.

My parents taught me perseverance and dedication, but above all that the best kind of knowledge to learn is for own's sake.

Nothing is unachievable; largest task can be accomplished by taking one step at a time.

Contents

LIST OF FIGURES	xvi
LIST OF TABLES	xvii
ACKNOWLEDGEMENTS	xix
ABSTRACT	xxi
1 INTRODUCTION: A REVIEW OF SILICON PHOTOVOLTAIC CELLS	1
1.1 Brief History of Solar Cells	4
1.2 Generation of Solar Cells	6
1.2.1 First Generation Solar Cell	7

1.2.2	Second Generation Solar Cell	8
1.2.3	Third Generation Solar Cell	10
1.3	Introduction to Nanostructured Solar Cells	11
1.4	Loss Mechanisms in Solar Cells	14
2	FUNDAMENTALS OF ELECTRON TRANSITION, AND TRANSITION PROB-	
	ABILITY	21
2.1	Introduction	21
2.2	Interaction of Photon with an Electron	22
3	ABSORPTION OF PHOTONS IN NANOSTRUCTURES	33
3.1	Introduction	33
3.2	Intra-band Absorption of Photons	34
3.2.1	Direct Band Gap Transition	34
3.2.1.1	Allowed Term in Matrix Element H_{m0}	37

3.2.1.2	Forbidden Term in Matrix Element H_{m0}	42
3.2.2	Indirect Band Gap Transition	43
3.3	Exciton Level Electron Transition	46
3.4	DOS, and Fermi Energy Dependence	48
3.5	Photoluminescence (PL)	51
4	RESULTS AND DISCUSSION FOR ABSORPTION COEFFICIENT AND PHOTOLUMINESCENCE	53
4.1	Refractive Index	54
4.2	Intra-band Absorption of Photons	56
4.2.1	Direct Band Gap Transition	57
4.2.2	Indirect Band Gap Transition	62
4.2.3	Exciton Level Electron Transition	63
4.3	Photoluminescence (PL)	64

5	COMPARISON OF ABSORPTION COEFFICIENT WITH SOLAR CELL EFFICIENCY	69
5.1	The Solar Cell Structure Design	70
5.2	Photocurrent in the Solar Cell	71
5.3	Practical Efficiency Calculations	74
6	CONCLUSION AND FUTURE WORK	77
A	MATHEMATICAL PROOFS	79
A.1	Shockley-Queisser Limit	79
B	PHYSICAL PROOFS	83
B.1	Quantum Confinement in Silicon Quantum Dot Structures	83
C	PERMISSION FOR IMAGE REPRINT	87
C.1	Chapter 1: 1	87

BIBLIOGRAPHY	91
---------------------	-----------

INDEX	95
--------------	-----------

List of Figures

1.1	The "solar tree", a symbol of Gleisdorf. Permission: Appendix C.1	2
1.2	The solar radiation spectrum at earth's sea level, and top of atmosphere. Image created by Robert A. Rohde / Global Warming Art. Permission: Appendix C.1	3
1.3	Photovoltaic World production with the line showing the best-fit exponential to the production for the most recent 10 years, indicating a doubling of production every 2 years. Plot by Geoffrey A. Landis. Permission: Appendix C.1	5
1.4	Solar cell efficiency for various generation solar cell. Source: NREL. Permission: Appendix C.1	7
1.5	Current standing of third generation w.r.t. other generations. Source: Source: SPREE, UNSW. Permission: Appendix C.1	12

1.6	Schematic of a tandem solar cell. Source: SPREE, UNSW. Permission:	
	Appendix C.1	13
1.7	Schematic of an all-Silicon Tandem Cell incorporating the quantum struc-	
	tures.	13
1.8	Loss Processes in a Solar cell [1]. Source: SPREE, UNSW. Permission:	
	Appendix C.1	14
1.9	Density of states for electrons in bulk semiconductors (3D; in blue), quan-	
	tum wells (2D; red), quantum wires (1D; green) and quantum dots (0D;	
	black)	15
1.10	Hot Carrier Solar Cell Schematic	18
2.1	Plot for $\frac{\sin^2 xt}{(xt)^2}$, as in equation (2.16). This is used to define transition prob-	
	ability.	29
3.1	E-k diagram for photon induced direct-gap electron transition	35
3.2	E-k diagram for photon induced indirect-gap electron transition. Shows	
	two possible mechanisms for electron to transit between states 0 and m , via	
	intermediate state I_v or I_c	44

3.3	Variation of band structure due to exciton formation. Shows the coulombic attraction between the electron-hole pair	47
3.4	Fundamental Absorption Edge in a heavy n-doped (n^+) doped material. Shaded region depicts fully filled energy levels. The fermi level ξ_f lies in the conduction band.	50
4.1	Variation of Refractive Index η (y-axis) with the wavelength λ (μm) of incoming photon	56
4.2	Comparison of absorption coefficient α , for allowed and forbidden transition for a 9:1 probability	59
4.3	Variation of Absorption coefficient α for direct band gap transition, for photons with varying incoming wavelength λ , and for a array of Silicon QDs of varying band gap ξ_g , for dots under quantum confinement	60
4.4	$n = 5$ exciton states binding energy variation with wavelength	64
4.5	Comparative plots for exciton and direct gap absorption, keeping all other parameters same. The band gap varies from $1.12 eV$ to $3.65 eV$	65
4.6	Exciton absorption curve showing the resonance peaks for $n = 5$ possible states, for $\xi_g = 1.69 eV$	66

4.7	The highlighted curve shows the actual PL spectra expected, as the electron while transiting will not occupy all the states	67
4.8	Absorption Coefficient Curve for Silicon Bulk Solar Cells of 1 st Generation, plotted for allowed terms from section 4.2.2	68
5.1	Schematic of a $p^+ - i - n^+$ designed solar cell structure	71
5.2	Energy band diagram of the $p^+ - i - n^+$ solar cell shown in figure 5.1 . . .	72
B.1	Band Gap for Silicon Quantum Dots' calculated by EMA Approximation .	86

List of Tables

1.1	Current Generation Solar Cell Approaches	19
3.1	Band-to-Band Transition	45
5.1	Parameter Values for short circuit current in intrinsic region	75

Acknowledgments

I would like to thank Dr Anand K. Kulkarni for being my advisor and giving me the opportunity to work on such an exciting and upcoming field. Dr. Kulkarni's perpetual energy and guidance had motivated me to perform and think out of the box. He had always been accessible, and more than willing to discuss and help with the research. His flair for in-depth analysis, and thinking beyond the obvious kept me disposed towards the research.

I am obliged to Dr. Paul Bergstrom, Dr. Max Seel, both at Michigan Tech, and Dr. Gavin Conibeer at University of New South Wales for their time. I had groundbreaking conversations and discussion related to my project, and their guidance has helped me a lot in streamlining the efforts for the research. I would also like to thank Dr. Harry Atwater at Caltech, whose work in the same field helped me working efficiently on my project. I am thankful to Dr. Paul Bergstrom and Dr. Stepher Hackney for serving on my committee.

My parents have been utmost supporting, and were by my side through the ups and the downs. They provided me with the best possible environment to grow up, and prosper as an individual. I am out of words to describe their everlasting love for me. This thesis would not have been possible without their never-ending care and affection.

I would like to show my gratitude to my colleagues, Ghous, Daw Don, Alex, and others who have been of been real help, and made it very convivial for me to work on the project.

A special thanks to Vidur Parkash, who in a few months will receive a doctorate himself, for all the time we spent in discussing the trivialities of my research. He has been a great friend, but also an inspiring mentor, who kept me driven towards the final destination.

God has been my witness in all the tests that I cleared in my life. May your name be exalted, honored, and glorified.

Abstract

Renewable energy is growing in demand, and thus the the manufacture of solar cells and photovoltaic arrays has advanced dramatically in recent years. This is proved by the fact that the photovoltaic production has doubled every 2 years, increasing by an average of 48% each year since 2002.

Covering the general overview of solar cell working, and its model, this thesis will start with the three generations of photovoltaic solar cell technology, and move to the motivation of dedicating research to nanostructured solar cell. For the current generation solar cells, among several factors, like photon capture, photon reflection, carrier generation by photons, carrier transport and collection, the efficiency also depends on the absorption of photons. The absorption coefficient, α , and its dependence on the wavelength, λ , is of major concern to improve the efficiency. Nano-silicon structures (quantum wells and quantum dots) have a unique advantage compared to bulk and thin film crystalline silicon that multiple direct and indirect band gaps can be realized by appropriate size control of the quantum wells. This enables multiple wavelength photons of the solar spectrum to be absorbed efficiently.

There is limited research on the calculation of absorption coefficient in nano structures of silicon. We present a theoretical approach to calculate the absorption coefficient using quantum mechanical calculations on the interaction of photons with the electrons of the valence band. One model is that the oscillator strength of the direct optical transitions is

enhanced by the quantum confinement effect in Si nanocrystallites. These kinds of quantum wells can be realized in practice in porous silicon. The absorption coefficient shows a peak of 64638.2 cm^{-1} at $\lambda = 343 \text{ nm}$ at photon energy of $\xi = 3.49 \text{ eV}$ ($= 355.532 \text{ nm}$). I have shown that a large value of absorption coefficient α comparable to that of bulk silicon is possible in silicon QDs because of carrier confinement. Our results have shown that we can enhance the absorption coefficient by an order of 10, and at the same time a nearly constant absorption coefficient curve over the visible spectrum. The validity of plots is verified by the correlation with experimental photoluminescence plots. A very generic comparison for the efficiency of p-i-n junction solar cell is given for a cell incorporating QDs and sans QDs. The design and fabrication technique is discussed in brief. I have shown that by using QDs in the intrinsic region of a cell, we can improve the efficiency by a factor of 1.865 times. Thus for a solar cell of efficiency of 26% for first generation solar cell, we can improve the efficiency to nearly 48.5% on using QDs.

Chapter 1

INTRODUCTION: A REVIEW OF SILICON PHOTOVOLTAIC CELLS

The reciprocal of electroluminescence is the photovoltaic effect, wherein the radiation is converted to electrical energy. Solar cells convert the sunlight energy directly to electricity. Renewable energy is growing in demand, and thus the manufacture of solar cells and photovoltaic arrays has advanced dramatically in recent years. Photovoltaic technology is the world's fastest growing renewable energy technology, and is proved by the fact that the photovoltaic production has doubled every 2 years, increasing by an average of 48 percent each year since 2002. Figure 1.1 shows the commercial use of solar panels to generate street electricity in the city of Gleisdorf in Austria.



Figure 1.1: The "solar tree", a symbol of Gleisdorf. Permission: Appendix C.1

Earth's atmosphere is showered with 120,000 TW of power in form of photons in a day. Using only 10% efficient solar cells, we can generate 20 TW of energy by only covering 0.16% of earth surface ($148,940,000 \text{ km}^2$) [2]. This energy will be twice the amount of energy burnt in fossil fuels. The other way to put this is that only 1/10000 of the sunlight reaching earth's surface is enough to provide energy for the humankind. The solar spectrum is shown in figure 1.2, with curves depicting black body radiation. Giacomo Ciamician in his lecture on *Photochemistry of the Future*, said [3]

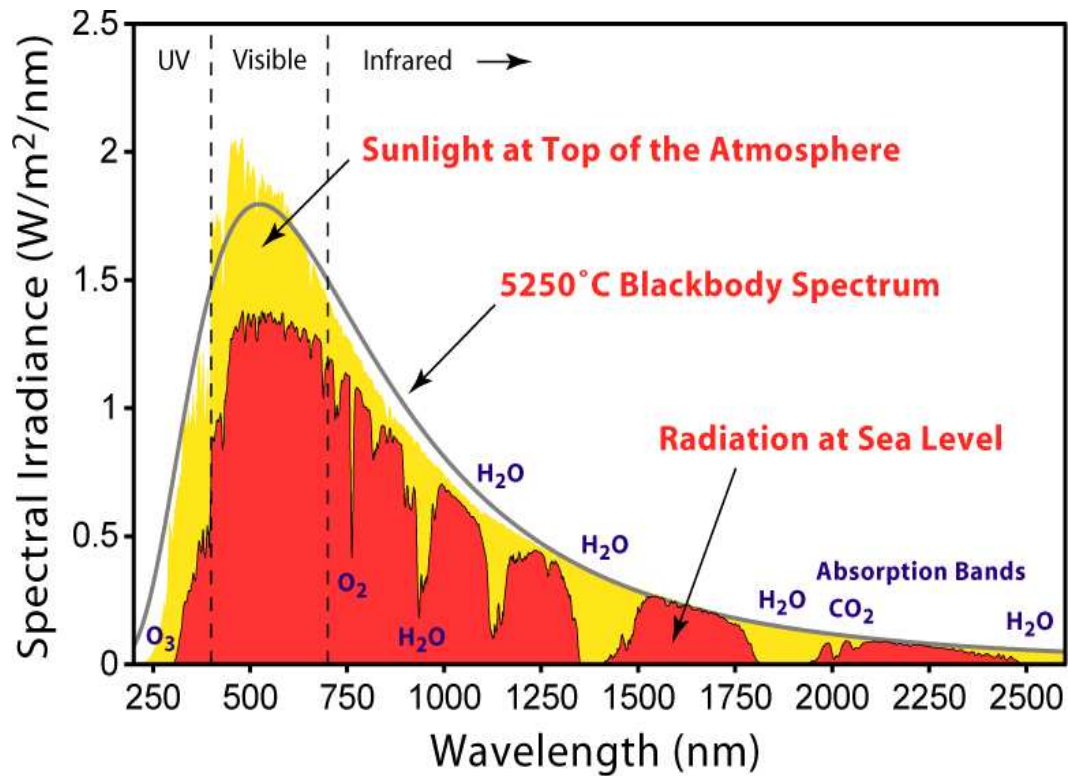


Figure 1.2: The solar radiation spectrum at earth's sea level, and top of atmosphere. Image created by Robert A. Rohde / Global Warming Art. Permission: Appendix C.1

So far human civilization has made use almost exclusively of fossil solar energy. Would it not be advantageous to make a better use of radiant energy?... Solar energy is not evenly distributed over the surface of the earth. There are privileged regions, and others that are less favored by the climate. The former ones would be the prosperous ones if we should become able to utilize the energy of the sun. ... If our black and nervous civilization, based on coal, shall be followed by a quieter civilization based on the utilization of solar energy, that will not be harmful to the progress and to human happiness.

1.1 Brief History of Solar Cells

It was in the year 1839, that Photovoltaic effect was first recognized by French physicist Alexandre-Edmond Becquerel. He noted that electric current was produced by the absorption of light on the silver coated platinum electrode immersed in an electrolyte. It took more than 40 years for the first practical solar cell to be realized, when in 1883 Charles Fritts formed a solar cell by coating the semiconductor selenium with an extremely thin layer of gold to form the junctions. These solar cells were nearly 1 % efficient.

In the year 1946, Russell Ohl patented his device as a solar cell under patent US2402662 for Light sensitive device. In the 1950s, the development of silicon electronics paved the way for p-n junctions. Bell Laboratories, experimenting with semiconductors, accidentally found that silicon doped with certain impurities was very sensitive to light. Thus, the first silicon solar cell was reported by Chaplin, Pearson and Fuller in the year 1954, with an efficiency of 6 %. This number increased with time, but the cost of production of energy (around \$200 per Watt) hindered the research in this field. During this time, other materials such as Cadmium Sulphide, Gallium Arsenide, Indium Phosphide, and Cadmium Telluride were studied as they promised better efficiency than silicon. However, silicon prevailed and still remains the most important photovoltaic material, because of its abundance, and also because of the fact that industry is more silicon technology based.

The 1973 Oil Embargo triggered the crisis in energy supply, and the non-oil supplying

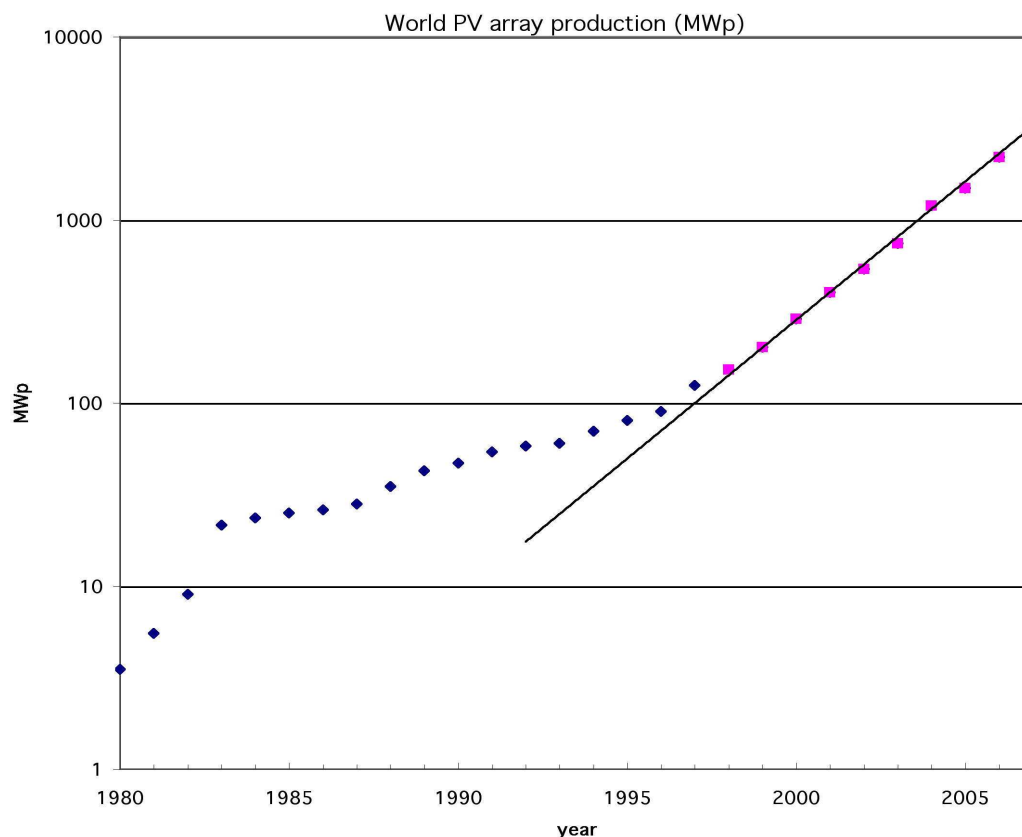


Figure 1.3: Photovoltaic World production with the line showing the best-fit exponential to the production for the most recent 10 years, indicating a doubling of production every 2 years. Plot by Geoffrey A. Landis. Permission: Appendix C.1

countries started looking at alternate sources of fuels, more particularly the renewable energy. Solar photovoltaic research gained momentum as funding for research and development increased. As a gesture of promoting solar energy incentive, President Jimmy Carter installed solar panels on the White House in the year 1977. By the end of 1980, the total world production of photovoltaic cells power had exceeded 600 kW. Since the cost of production per watt was very high at this point, there wasn't a widespread commercial development of solar cell technology. But still a lot of improvement in the cost factor had

been achieved as the price of photovoltaic energy was down from 100 US\$/watt in 1971 to 7 US\$/watt in 1985.

Interest in photovoltaic systems and technology kept on growing through the years. The economics of photovoltaics improved in late 1990s primarily through economies of scale, which was attributed to the expansion of 18-25 % per annum. By the late 1990s and early 2000s, solar cell technology was being used for remote low power applications such as navigation, telecommunication, space satellites and rural electrification [4]. The plot in figure 1.3 shows doubling in production of PV energy over the last 10 years or so. As the technology of manufacturing solar cells changed, so did the generations of solar cells have. With certain advantages and disadvantages over previous generation, the generation of solar cells have been discussed in brief in the following section.

1.2 Generation of Solar Cells

As with the growth in semiconductor industry, the solar cells have moved through generations, viz. three which have made impact on the solar cell industry. The salient features of these generations are listed below. There is continual effort and research conducted in all the three generations of solar cell to improve the efficiency and cost of per watt of generated power.

1.2.1 First Generation Solar Cell

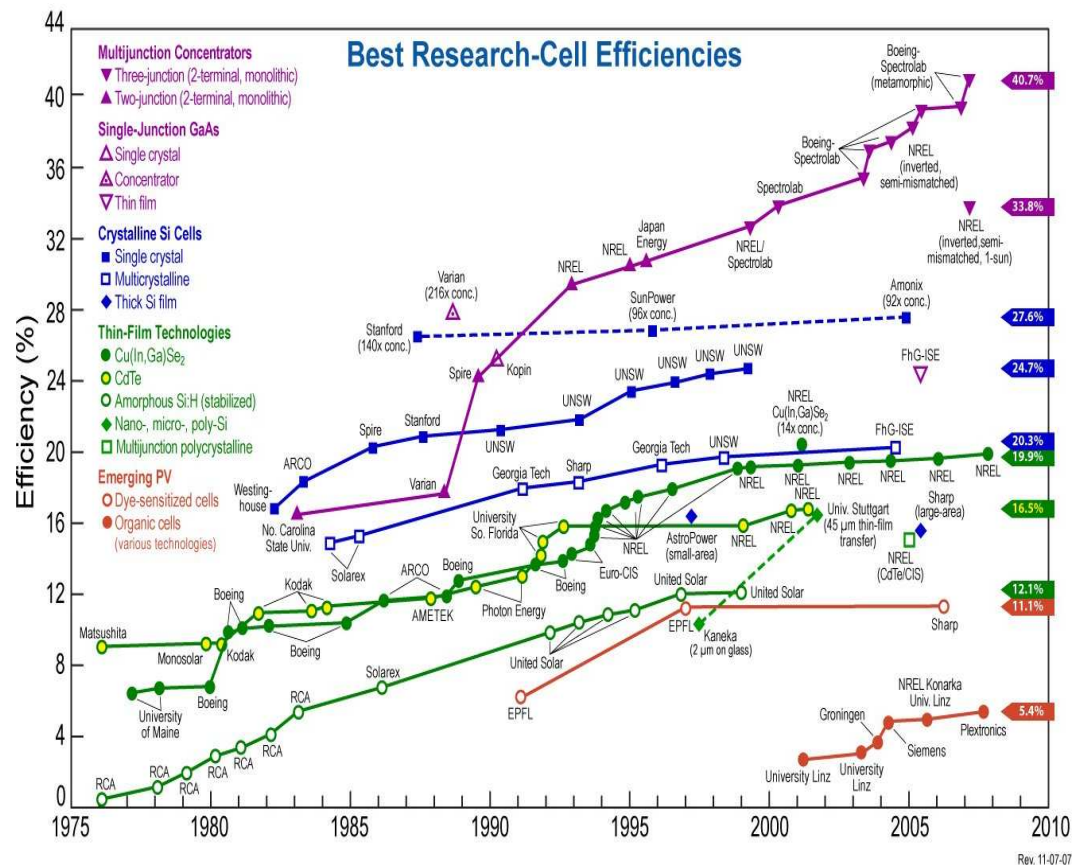


Figure 1.4: Solar cell efficiency for various generation solar cell. Source: NREL.
Permission: Appendix C.1

The first generation solar cells are mono crystalline silicon-based, bulk solar cells. These are basically high quality, single p-n junction based devices. The production cost for this generation is high owing to the technologies involving high energy, and high inputs of labor. The current solar cell efficiency for first generation solar cell is 27.8 %, which is fast approaching the theoretical limit of 31 % [5] as described by Shockley-Queisser limit for single junction device. For more on the Shockley-Queisser limit, please refer to the

section on Mathematical Proofs. Even with the high cost per watt of generated energy, first generation solar cells are most highly commercially produced solar cells, owing to the high efficiency of these cells. They account for nearly 89.6% of the commercially produced solar cell market. One of the most recent approach which saves energy is to process discrete cells on silicon wafers cut from multicrystalline ribbons [6].

The efficiency for first generation solar cells is shown in Figure 1.4 for crystalline silicon cells. The single crystal solar cell is reaching the stagnation point, and is currently 24.7 % efficient. Even the concentrator solar cells using microcrystalline silicon, is nearly at the edge of Shockley-Queisser limit for single gap silicon solar cell, and is 27.6 % efficient.

1.2.2 Second Generation Solar Cell

The Second Generation Solar cells came into the market to remedy the high cost of production for the first generation solar cell. These were basically the thin-film solar cells, which were significantly cheaper to produce than their first generation counterparts. But the gain in cost of production was at the expense of efficiency of the solar cell, which was reduced. Another added advantage of second generation solar cell was their flexibility. The thin-film technology made way for solar panels of light weight and flexible texture, that could be rolled out on a roof, or any other surface. Research is being conducted to improve the efficiency, and once achieved, second generation solar cell will beat the first generation

solar cell owing to the lesser cost of production.

The most successful second generation solar cell materials have been cadmium telluride (CdTe), copper indium gallium selenide (CIGS), amorphous silicon (aSi:H) and micromorphous silicon. Instead of using wafers of silicon as the base, these materials are deposited on glass or ceramic surfaces to reduce the cost of the materials used. The trend of commercialization is increasing towards second generation solar cell, which is only obstructed by the low efficiency of these cells, and hence the cost of production. But recently, a major manufacturer for this generation solar panels, *First Solar* based in Tempe, AZ, reported that it had reached the important *industry milestone* of reducing the cost of generated power to less than \$1 a watt. In a statement at the SPIE Conference at San Diego in 2009, First Solar, which has produced modules for solar installations in several countries in Europe, said it had brought costs down to \$1 from \$3. Other companies such as *Wurth Solar* and *Nanosolar* commercialized the CIGS technology, with a combined production of nearly 450 MW for the year 2008.

The thin film technology for solar cell production has been researched into a lot, and is still continuing. Referring to figure 1.4, CIGS solar cells produced in the labs by NREL are 19.9 % efficient. Even the CdTe solar cells are showing improvement, and with an efficiency of 16.5 % is one of the sought after materials for thin film solar cells. In fact, a thin film based heterojunction based CdS/CdTe is one of the most promising candidates among photovoltaic structures [7].

1.2.3 Third Generation Solar Cell

The Third Generation or the current generation solar cells came into research to overcome the high cost of production (first generation), and low efficiency (second generation) at the same time. This generation is still in the infant stages, and is very much research oriented. The current generation solar cells are very different in approach as compared to their counterparts, as they do not rely on traditional p-n junctions to separate the photogenerated charge carriers. Third generation contains a wide range of solar cell categories, including polymer solar cells, nanocrystalline cells, and dye-sensitized solar cells. Study of each category is a research based field.

Figure 1.4 shows the growth of efficiency with time for third generation solar cells. The multijunction solar cells incorporating nanostructures are still very much research based, and are hence not shown in this figure. They offer the promise of high efficiency solar cells with lower cost factors, and hence have the ability to overcome the existing efficiency and cost drivers. Having said that, the nanostructured solar cells have substantial challenges. The foremost challenge is that nanostructured solar cells have a surface area smaller as compared to their counterparts. Hence even with higher absorption coefficient for each heterostructure, the amount of absorption is less, and hence lesser is the collection, voltage and Fill Factor (FF). Also, even the most carefully grown heterostructure solar cells, using MBE (Molecular Beam Epitaxy), have efficiency lower than the same structures without nanostructures.

In this thesis, we will concentrate on nanocrystalline cells. This is an approach to circumvent the Shockley-Queisser limit for a single energy threshold material. This is done by creating multiple bandgaps using either multijunction photovoltaic cells, concentration of the incident spectrum, or thermal generation by UV light to enhance carrier collection. Creation of multiple band gaps improves the amount of energy, or photons absorbed. A solar cell company in the United Kingdom, Quanta Sol Ltd., recently announced an improvement in solar cell efficiency using quantum well structures [8]. They cite the enhancement of optical absorption in the quantum wells as the criteria for improvement of solar cell electrical characteristics, and hence its efficiency. The third generation solar cell aims to achieve conversion efficiencies of 30-60 %, while retaining low cost materials and manufacturing techniques [9, 1]. The current research for third generation solar cells is to improve the efficiency while keeping the cost low as shown in figure 1.5.

1.3 Introduction to Nanostructured Solar Cells

The silicon nanostructures are proposed for the next generation photovoltaic cells with increased device efficiencies. There have been many proposed models for next generation solar cell, wherein the electron confinement in a silicon based quantum dot heterostructure is proposed [1]. In such kinds of devices, the wide gap materials are being used as upper cell elements in silicon based tandem cells, as shown in figure 1.6, 1.7.

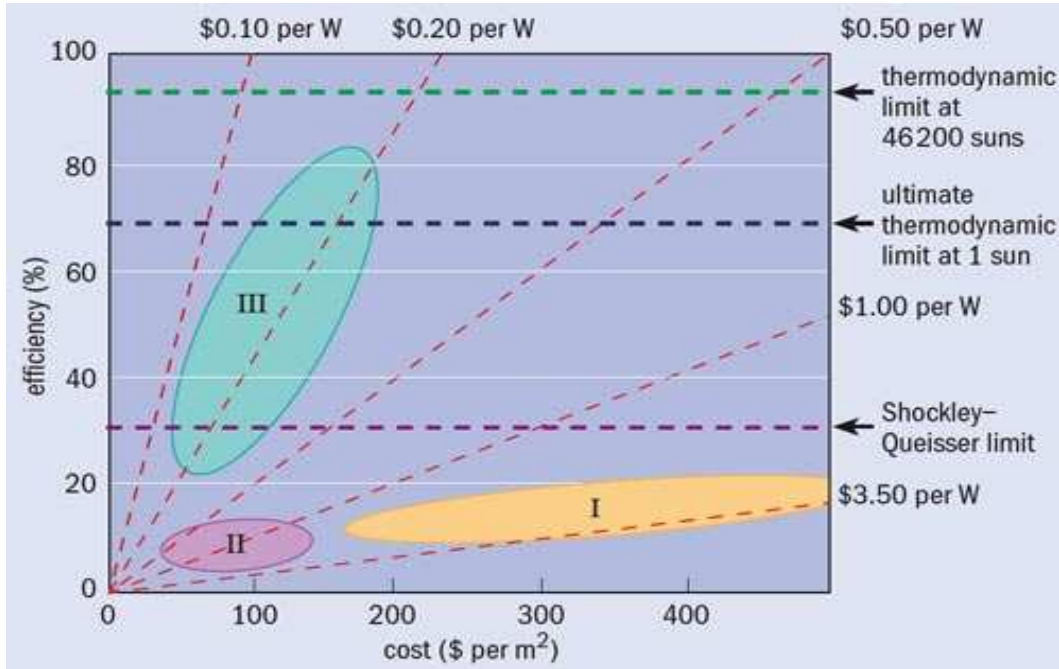


Figure 1.5: Current standing of third generation w.r.t. other generations. Source: Source: SPREE, UNSW. Permission: Appendix C.1

The aim of these next generation cells is to reduce the cost per watt over the previous generation "*thin film*" solar cells, by increasing the efficiency of the devices with only a small increase in the cost of the area [6]. These effects of increased efficiency (nearly 30-60 % [9]) and low cost thin film processes have the potential to reduce costs per peak watt of generating capacity very significantly to less than \$1 and below. To achieve such improvements in the efficiency, the Shockley-Queisser limit for single band gap materials [5] must be bypassed somehow. One way to do this is to have multiple energy threshold devices, as is the case of the tandem solar cells. There is a significant scope to investigate the feasibility of heterostructure based device, to achieve the multiple energy threshold devices [6, 4].

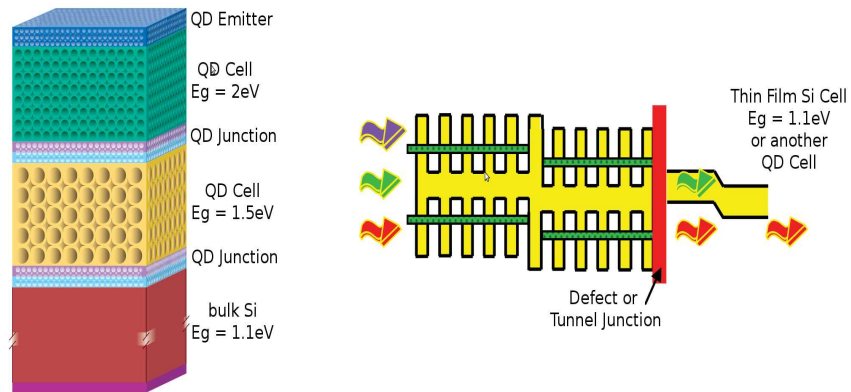


Figure 1.6: Schematic of a tandem solar cell. Source: SPREE, UNSW. Permission: Appendix C.1



Figure 1.7: Schematic of an all-Silicon Tandem Cell incorporating the quantum structures.

1.4 Loss Mechanisms in Solar Cells

The first and the second generation solar cells have a number of power loss mechanisms [1], of which the two most important that add up to the loss of nearly half of the incident solar energy are the inability of the cells to absorb photons with energy lesser than the band gap, and the lattice thermalization loss owing to the photons with energy more than the band gap [1, 6]. Referring to figure 1.8, one can see that for photons with energy less than the band gap are not absorbed by the material. For silicon, with a bulk band gap of $E_g = 1.12 \text{ eV}$, all photons with wavelength higher than nearly 1100 nm are not absorbed.

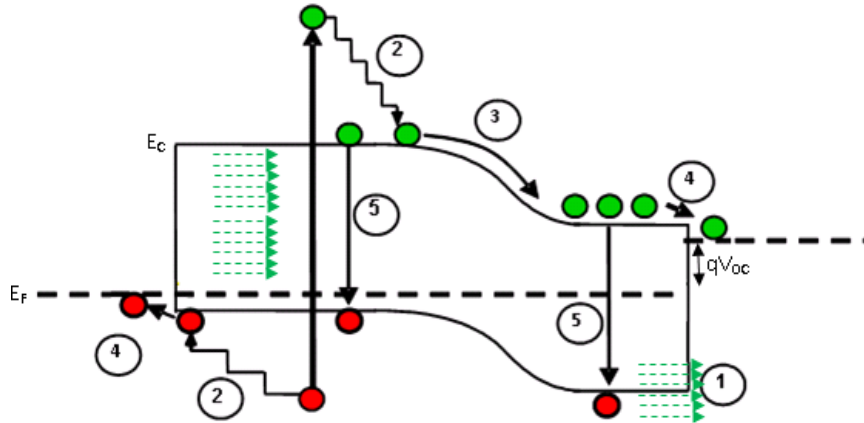


Figure 1.8: Loss Processes in a Solar cell [1]. Source: SPREE, UNSW. Permission: Appendix C.1

An attempt is made in this thesis, to increase the number of band gaps through application of nano-structures for silicon that exhibit quantum confinement effect. For any semiconductor nanocrystal, its properties depend upon quantum confinement, and therefore upon dots geometry and symmetry. A brief study of quantum confinement in Silicon Quantum

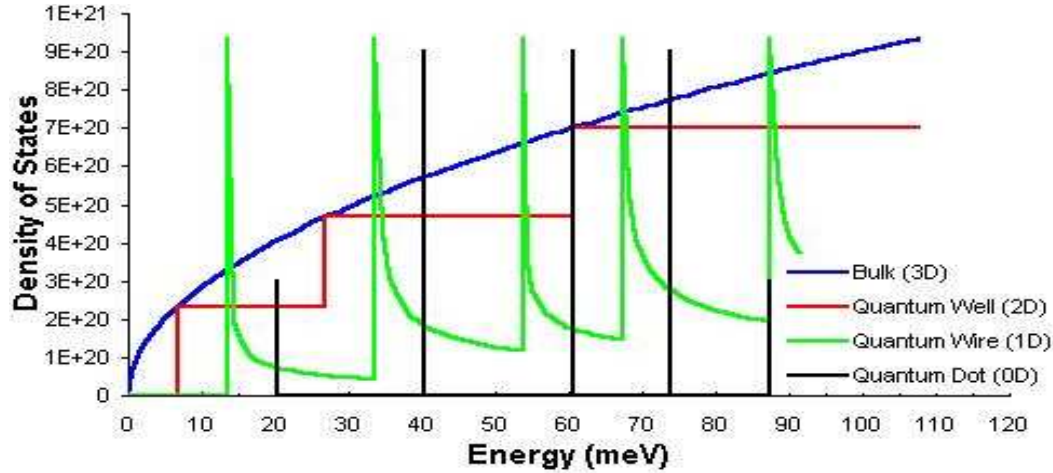


Figure 1.9: Density of states for electrons in bulk semiconductors (3D; in blue), quantum wells (2D; red), quantum wires (1D; green) and quantum dots (0D; black)

Nanostructures is given in B.1. The discreteness of density of states (DOS) in a quantum dot (QD) allows it to exhibit strong quantum confinement of free carriers. The variation of DOS w.r.t. dimension is shown in figure 1.9.

Whenever light is incident on a semiconductor, the phenomena of absorption, reflection and transmission are observed. Observing these three phenomena, one can obtain information on the band structure and electronic properties of semiconductor. To understand the absorption process at quantum level, we need to understand the physics behind the photon-electron interaction in a heterostructure. Figure 1.8, it shows the standard solar cell loss processes. These are [1]:

1. Non-absorption of photons with energies less than band gap energy
2. Lattice thermalization loss

3. Junction voltage loss
4. Contact voltage loss
5. Recombination loss

Many steps have been proposed to overcome and tackle these losses for the next generation solar cell. The applications to oversee these steps are discussed in brief in next paragraph. These steps are:

1. Increasing the number of bandgaps
2. Capture carriers before thermalization
3. Multiple carrier pair generation per high energy photon (or the other way can be single carrier pair generation with multiple low energy photons)

The next generation solar cells aim to control the above losses by the approach of multiple threshold band gaps. Tandem solar cell is one of the examples for multiple threshold approach, which exceed the Shockley-Queisser limit. Single p-n junction based nanostructured solar cells have been proposed, with the use of quantum well or inter-penetrating networks of quantum dots [10], or quantum dot solar cells. All of these proposals essentially increase the number of band gaps. There have been efforts to increase the number of bandgaps by fabricating a tandem cell based on silicon and its oxides and nitrides using reduced dimension silicon nanostructures to engineer the band gap of an upper cell material

[1]. Efforts are also being made to see if the other proposed steps enumerated above can be worked out. This is being done by investigating the "Hot Carrier solar cell", schematic shown in figure 1.10, in which carrier cooling is slowed such that carriers can be extracted before thermalization. This requires both an absorber with slowed carrier cooling properties and collection of carriers over a limited range of energies, such that cold carriers in the external contacts do not cool the hot carriers to be extracted [1]. Hot electrons in the conduction band are extracted before they thermalize, resulting in increased photovoltage at the contacts and theoretical light-to-electricity conversion efficiency limits as high as 68% under one-sun illumination conditions can be achieved [11]. The strategy of multiple carrier generation is being looked into either by down-conversion in a layer on the front of the cell or by application of an up-converter to the rear of a Si cell. Rare earth doped phosphors in the up-converter absorb below band gap photons and up-convert two or more to above band gap photons which are then incident on the Si cell. All the current approaches to circumvent the Shockley-Queisser Limit have been summed up in table 1.1.

In this thesis, we will concentrate on only one of the aspects of improving the efficiency. Through application of multiple band gaps using quantum nanostructures of silicon, we will show improvement in absorption coefficient over second generation solar cell. Companies like Quanta Sol Ltd. have shown that the first generation of these quantum well photovoltaic cells have an efficiency of nearly 27% [8]. This is very close to the single p-n junction cell efficiency [5] of 31%. Adding to this is the fact that the processing steps for these solar cells have been the thin-film processes, and hence are low cost and ready for large

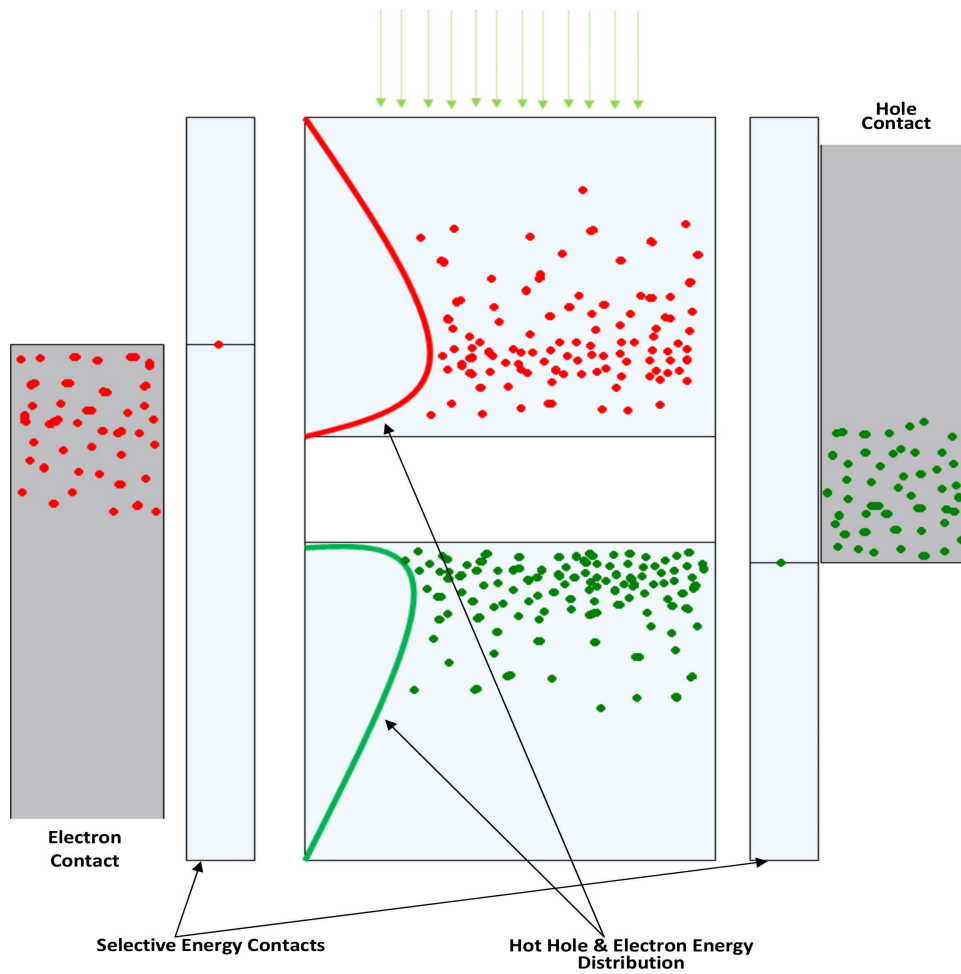


Figure 1.10: Hot Carrier Solar Cell Schematic

scale production. Introduction of quantum structures in solar cells increases the spectral range, and thus achieves high efficiency, with very low dislocations introduced in the crystal structure.

SHOCKLEY- QUEISSER AS- SUMPTION	APPROACH	EXAMPLE
One quasi-fermi level separation	MULTI-LEVEL ENERGY SOLAR CELLS - Have multi-levels for metastable generated carriers	Tandem Solar Cells using QDs, Intermediate band Quantum Wells Solar Cells such as SQWC
One photon gener- ates one $e^- - h^+$ pair	SOLAR CELLS WITH MULTIPLE ABSORPTION PATHS - Multiple carrier pair generation per high en- ergy photon, or single carrier pair generation for many low energy photons	Impact Ionization, 2-Photon Absorp- tion
$T_{Carrier} = T_{Cell}$	SOLAR CELLS CAPTURING CARRIERS BEFORE THERMAL- IZATION - Energy is extracted from a difference in carrier and lattice temperature	Hot Carrier Solar Cells
Solar Spectrum In- put	MULTI-SPECTRUM SOLAR CELLS - Conversion of input spectrum to narrower wavelength range with same energy profile	Up/Down Conver- sion

Table 1.1: Current Generation Solar Cell Approaches

Chapter 2

FUNDAMENTALS OF ELECTRON TRANSITION, AND TRANSITION PROBABILITY

2.1 Introduction

The properties for any nanostructured semiconductor, its properties depend upon quantum confinement, and therefore upon its geometry and symmetry. The discreteness of density of states (DOS) in a quantum structure, confined in certain dimensions, allows the structure to exhibit strong quantum confinement. Whenever light is incident on a semiconductor, the

phenomenon of absorption, reflection and transmission are observed. Observing these three phenomena, one can obtain information on the band structure and electronic properties of semiconductor.

For understanding the process of photons' absorption in the quantum structures, we use a mathematical model for interaction of photon with an electron [12], with structures under quantum confinement. Once we have this model, we can relate the optical absorption coefficient α with the findings of this model, viz. the transition probability of an electron, and the band structure of the nano particles used.

To define the model, we summarize below the quantum mechanical equations [12, 13] associated with it. Thereon as we progress, absorption coefficient for various cases discussed in chapter 1, is derived from this mathematical model.

2.2 Interaction of Photon with an Electron

Photon is defined by a vector potential \vec{A} , which is assumed to be a planar wave, given by,

$$\vec{A} = \frac{1}{2}A\hat{a}\exp[i(\vec{q}\cdot\vec{r}-t\omega)] + \frac{1}{2}A\hat{a}\exp[i(\vec{q}\cdot\vec{r}+t\omega)] \quad (2.1)$$

\hat{a} is the unit polarization vector in the direction of \vec{E} , which is defined as the Maxwell equa-

tions for the above vector potential. \vec{q} is defined as the wavevector of the photon. For above equation (2.1), the first term on the right hand side corresponds to the stimulated absorption, and the second term denotes the stimulated emission. The magnitude of wavevector of a photon \vec{q} , is related to its frequency by,

$$|\vec{q}| = \frac{\omega\eta}{C}$$

C is the velocity of light, and η is the refractive index of the material being used for photon absorption.

The vector potential (2.1) obeys the Maxwell Equation given as,

$$\vec{E} = -\frac{\partial}{\partial t}\vec{A} \tag{2.2}$$

$$\mu\vec{H} = \vec{\nabla}_r \times \vec{A} \tag{2.3}$$

$$\vec{\nabla}_r \cdot \vec{A} = 0 \tag{2.4}$$

By the virtue of being electromagnetic plane wave, the photon's unit polarization vector follows the relation,

$$\hat{a} \cdot \vec{q} = 0$$

The classical Hamiltonian for interaction of a photon of vector potential \vec{q} with an electron of wavevector \vec{k} is given by

$$\vec{H} = \frac{1}{2m}(\hbar\vec{k} - e\vec{A})^2 = \frac{1}{2m}(\hbar^2\vec{k}^2 - \hbar e\vec{k} \cdot \vec{A} - \hbar e\vec{A} \cdot \vec{k} + e^2\vec{A}^2) \quad (2.5)$$

For low light levels, we can easily ignore the term containing the square of the vector potential of photon, i.e. the \vec{A}^2 term, without any loss of generality. Using the low light assumption, and the operator form of \vec{k} ($= i\vec{\nabla}_r$), we can write the above equation (2.5) as

$$\vec{H} = \frac{1}{2m}(-\hbar^2\vec{\nabla}_r^2 + i2\hbar e\vec{\nabla}_r \cdot \vec{A}) = \frac{-\hbar^2}{2m}\vec{\nabla}_r^2 + \frac{ie\hbar}{m}\vec{A} \cdot \vec{\nabla}_r \quad (2.6)$$

The first term of above equation (2.6) is the unperturbed electron energy, and is denoted by \vec{H}_0 . The second term, denoted by \vec{H}' is the energy term due to photon-electron interaction. We will solve the time-dependent Schrödinger equation for this because the interaction of

photon and electron results in a change of state for the electron with time. Thus we get the following equation:

$$(\vec{H}_0 + \vec{H}')\Psi = i\hbar \frac{\partial \Psi}{\partial t} \quad (2.7)$$

We solve for the above equation (2.7) by assuming the solutions to be a linear combinations of the wavefunctions Ψ_n for the unperturbed time-independent system, with

$$\Psi = \sum A_n(t) \Psi_n \exp\left(\frac{-i\xi_n t}{\hbar}\right) \quad (2.8)$$

Here ξ_n satisfies the the unperturbed Schrödinger equation $\vec{H}_0 \Psi_n = \xi_n \Psi_n$. Solving equations (2.7) and (2.8), we obtain

$$\sum A_n (\vec{H}_0 \Psi_n + \vec{H}' \Psi_n) \exp\left(\frac{-i\xi_n t}{\hbar}\right) = \sum (A_n \xi_n + i\hbar \frac{dA_n}{dt} \Psi_n) \exp\left(\frac{-i\xi_n t}{\hbar}\right)$$

Using the unperturbed Schrödinger equation with the above equation, we can see that the first term on the LHS is equal to the first term on the RHS. Thus, we can write

$$\sum A_n \vec{H}' \Psi_n \exp\left(\frac{-i\xi_n t}{\hbar}\right) = i\hbar \sum \frac{dA_n}{dt} \Psi_n \exp\left(\frac{-i\xi_n t}{\hbar}\right) \quad (2.9)$$

Multiply both side (2.9) with $\Psi_m^* \exp\left(\frac{i\xi_m t}{\hbar}\right)$, and integrate over the whole volume V of the crystal to get

$$\begin{aligned} & \sum_n A_n \vec{H}' \exp\left(\frac{i(\xi_m - \xi_n)t}{\hbar}\right) \int_V \{\Psi_m^* \vec{H}' \Psi_n d\mathbf{r} \\ &= i\hbar \sum \frac{dA_n}{dt} \exp\left(\frac{i(\xi_m - \xi_n)t}{\hbar}\right) \int \Psi_m^* \Psi_n d\mathbf{r} \end{aligned} \quad (2.10)$$

We know that that unperturbed wavefunctions are orthogonal, hence using $\int_V \{\Psi_m^* \vec{H}' \Psi_n d\mathbf{r} = N\delta_{mn}$ in equation (2.10),

$$i\hbar \frac{dA_m}{dt} = \sum_n A_n H_{mn}(t) \exp\left[\frac{i(\xi_m - \xi_n)t}{\hbar}\right] \quad (2.11)$$

Here $H_{mn}(t)$ is the electron transition matrix element to state m with energy ξ_m from state n with energy ξ_n , for a crystal matrix of N primitive unit cells. This matrix element is given by,

$$H_{mn}(t) \equiv \frac{1}{N} \int_V \{\Psi_m^* \vec{H}' \Psi_n d\mathbf{r}\}$$

The equation (2.11) is the differential form for the time-dependent coefficients of the function given in equation (2.8). We use first-order perturbation theory in order to solve for the coefficients A_m in equation (2.11). We solve for transition from state 0 to state m , starting at $t = 0$ with energy ξ_0 (with the assumption $A_0(t=0) = 1$ and $A_n(t=0) = 0$), to get,

$$\imath \hbar \frac{dA_m}{dt} = H_{m0}(t) \exp \left[\frac{\imath (\xi_m - \xi_0) t}{\hbar} \right]$$

Integrate this equation with respect to time, t , to get,

$$A_m(t) = \frac{1}{\imath \hbar} \int_0^t H_{m0}(t) \exp \left[\frac{\imath (\xi_m - \xi_0) t}{\hbar} \right] dt \quad (2.12)$$

To evaluate the value of equation (2.12), we need to evaluate the value of $H_{m0}(t)$, which is the unperturbed Hamiltonian for electron transition from state 0 to state m , and can be written using the matrix element equation as (\vec{A} is the photon vector potential as defined earlier),

$$H_{m0}(t) = \frac{\imath e \hbar}{mN} \int_V \{ \Psi_m^* (\vec{A} \cdot \nabla_r) \Psi_0 d\mathbf{r} \quad (2.13)$$

We can ignore the stimulated emission term in the equation (2.1), and use it to evaluate $(\vec{A} \cdot \nabla_r)$,

$$\begin{aligned} H_{m0}(t) &= \frac{\imath e \hbar A}{2mN} \exp(-\imath \omega t) \int_V \Psi_m^* \exp(\imath \vec{q} \cdot \mathbf{r}) (\hat{a} \cdot \nabla_r) \Psi_0 d\mathbf{r} \\ &= H_{m0} \exp(-\imath \omega t) \end{aligned} \quad (2.14)$$

The above equation now is separated in two terms; one independent of time - H_{m0} , and the time dependent term - $\exp(-\imath \omega t)$. Thus, we can write the equation (2.12), using (2.14) as,

$$\begin{aligned} A_m(t) &= \frac{H_{m0}}{\imath \hbar} \int_0^t \exp \left[\frac{\imath (\xi_m - \xi_0 - \hbar \omega) t}{\hbar} \right] dt \\ &= \frac{H_{m0}}{(\xi_m - \xi_0 - \hbar \omega)} \left\{ 1 - \exp \left[\frac{\imath (\xi_m - \xi_0 - \hbar \omega) t}{\hbar} \right] \right\} \end{aligned} \quad (2.15)$$

The transition probability for an electron to go from state 0 to state m is mathematically given as $|A_m(t)|^2$, which now can be evaluated from equation (2.15). The transition prob-

ability is thus

$$|A_m(t)|^2 = 4|H_{m0}|^2 \frac{\sin^2 \left[\frac{(\xi_m - \xi_0 - \hbar\omega)t}{2\hbar} \right]}{(\xi_m - \xi_0 - \hbar\omega)^2} = \frac{|H_{m0}|^2}{\hbar^2} \frac{\sin^2 xt}{x^2} \quad (2.16)$$

Here $x = \frac{\xi_m - \xi_0 - \hbar\omega}{2\hbar}$. The curve for the term $\frac{\sin^2 xt}{(xt)^2}$, is shown in figure 2.1

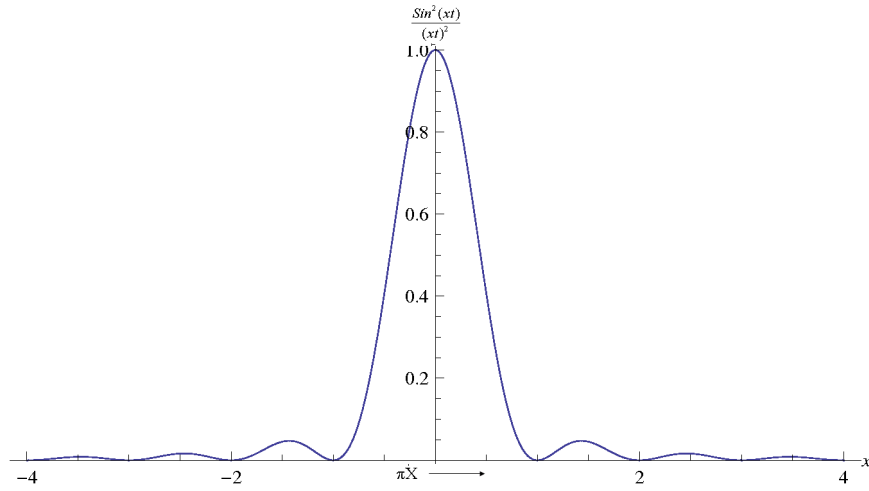


Figure 2.1: Plot for $\frac{\sin^2 xt}{(xt)^2}$, as in equation (2.16). This is used to define transition probability.

From figure 2.1 one can observe that the height of the term increases with time t (as t^2), whereas the width is inversely proportional to time t . The area under the curve is given by,

$$\int_{-\infty}^{\infty} \frac{\sin^2 xt}{(xt)^2} dx = \pi t$$

Using the above calculated area, we can make the approximation that for times sufficiently long for transition to take place,

$$\lim_{t \rightarrow \infty} \frac{\sin^2 xt}{(xt)^2} = \frac{\pi}{t} \delta(x)$$

$\delta(x)$ is the Dirac-Delta function [14]. We can now write the transition probability defined in equation (2.16), using the Dirac-Delta function as,

$$\begin{aligned} |A_m(t)|^2 &= \frac{\pi |H_{m0}|^2 t}{\hbar^2} \delta \left[\frac{(\xi_m - \xi_0 - \hbar\omega)}{2\hbar} \right] \\ &= \frac{2\pi |H_{m0}|^2 t}{\hbar} \delta(\xi_m - \xi_0 - \hbar\omega) \end{aligned} \quad (2.17)$$

Equation (2.17) shows us clearly that the probability for an electron to transit from state 0 with energy E_0 to a state m with energy E_m is zero unless the photon energy, $\hbar\omega$, is equal to the difference in energy between the states. This is basically the energy conservation in electron transition. The transition probability increases with time, t . The transition probability can be evaluated to a number, if the time-independent matrix element, H_{m0} can be solved and the value be known for a given transition. An electron of the valence band is promoted to an excited state in the conduction band that naturally decays to the bottom of the conduction energy band on a timescale of tens of picoseconds.

There are viz. three cases for a photon - electron interaction, and hence its absorption coefficient. For understanding purpose, let us assume direct - gap material with parabolic band structure. Foremost is the simple case when photon energy is equal to the energy band gap of the material used in solar cell. These photons will excite an electron from valence band to the lowermost level of conduction band. Second case is for photons with energy higher than the band gap; these will be absorbed by the material, with the transition of electrons from filled states in valence band to empty states in conduction band at higher levels. These electrons at higher state in conduction band will radiate energy in form of phonons, and de-excite to the lower levels of energy in conduction band. Lastly for photon energies just below the band gap energy, formation of excitons takes place, wherein the absorbed radiation transits the electron from filled valence band to impurity states. Such kind transition of free carriers produces a continuum of absorption which increases with decreasing photon energy. Crystal lattice also absorbs radiation wherein the energy is given off in optical phonons.

Chapter 3

ABSORPTION OF PHOTONS IN NANOSTRUCTURES

3.1 Introduction

In this chapter, the discussion focuses mainly on the possible three methods for absorption of photon in nanostructures. The nanostructures, due to their geometry and size, may exhibit direct bang gap, or indirect band gap features. Our results shown in next chapter, focuses mainly on nanostructures exhibiting strong quantum confinement, and hence direct band-gap behavior. Thus in these types of structures, there is de-localization of electrons, and hence the excitonic level absorption also presumes an importance at room temperatures.

The last section of this chapter discusses in brief the effects of Density of States (DOS) on absorption, and the effect of variation of Fermi Level Distribution on absorption coefficient. The last section is a classical approach to associate the absorption coefficient, α , and the photoluminescence spectra, PL .

3.2 Intra-band Absorption of Photons

In this section, the approach is taken to connect between the electron-photon interaction's transition probability, and the absorption coefficient α . The nanostructures can show band gap variation depending on the size, geometry of orientation of these nanostructures, which in turn defines the confinement. A number of processes have been discussed in previous chapter, through which an electron transition can take place. Efforts have been made to connect all the derivation, but at certain times, the things which are beyond the scope of this thesis, have been just referenced.

3.2.1 Direct Band Gap Transition

The assumption of parabolic band gap behavior has been taken to make the understanding of the situation, and the associated mathematical calculations easy. A typical energy $E - k$ diagram for direct gap materials is shown in figure 3.1. As photons with energy $\hbar\omega (> E_g$

band gap) shine on the material, the electron in valence band at state \mathbf{k} is excited to a state \mathbf{k}' in conduction band.

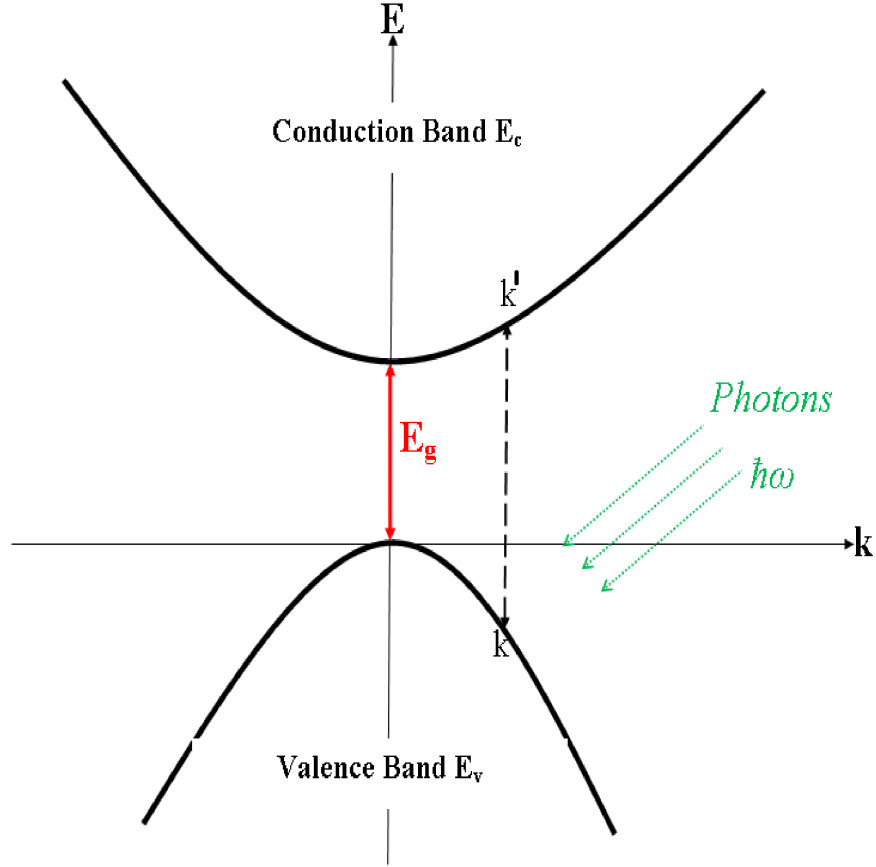


Figure 3.1: E-k diagram for photon induced direct-gap electron transition

The initial and final states for the transition of the electron in valence band at state \mathbf{k} is excited to a state \mathbf{k}' in conduction band, are only determined by the photon energy $\hbar\omega$. To get the value of transition probability, defined in (2.17), for this transition, the time - independent matrix element H_{m0} , defined in (2.13), has to be solved. For the transition considered, we can write the matrix element H_{m0} as,

$$\hbar_{k'k} = \frac{\imath \hbar e A}{2mN} \int_V \Psi_{k'}^* \exp(\imath \vec{q} \cdot \vec{r}) \left(\hat{a} \cdot \vec{\nabla}_r \right) \Psi_k d\mathbf{r} \quad (3.1)$$

$\Psi_{k'}^*$ and Ψ_k are the wavefunctions for the electron in the conduction band and the valence band respectively. According to Bloch's Theorem, these electron wavefunctions have the periodicity of direct lattice, and hence have the form,

$$\Psi_k = \exp(\imath \vec{k} \cdot \vec{r}) u_k(\mathbf{r})$$

$u_k(\mathbf{r})$ is strictly cell-periodic (of periodicity R) function such that $u(\mathbf{r}) = u(\mathbf{r} + \mathbf{R})$. Using the definition of wavefunction given above, we can write equation (3.1) as,

$$\begin{aligned} \hbar_{k'k} &= \frac{\imath \hbar e A}{2mN} \int_V \exp\left[\imath (\vec{k} - \vec{k}' - \vec{q}) \cdot \vec{r}\right] u_{k'}^* \left[\hat{a} \cdot \vec{\nabla}_r u_k + \imath (\hat{a} \cdot \vec{k}) u_k \right] d\mathbf{r} \\ &= \frac{\imath \hbar e A}{2mN} \sum_R \exp\left[\imath (\vec{k} - \vec{k}' - \vec{q}) \cdot \vec{r}\right] \int_{\Omega} u_{k'}^* \left[\hat{a} \cdot \vec{\nabla}_r u_k + \imath (\hat{a} \cdot \vec{k}) u_k \right] d\mathbf{r} \end{aligned}$$

If we have a closer look at the summation part in the above equation, we can easily see that for conservation of wavevector, the $\sum_R \exp\left[\imath (\vec{k} - \vec{k}' - \vec{q}) \cdot \vec{r}\right] = N$ (N is the primitive unit cells in the crystal). Thus above equation reduces to

$$\hbar_{k'k} = \frac{\imath \hbar e A}{2m} \int_{\Omega} u_{k'}^* \left[\hat{a} \cdot \vec{\nabla}_r u_k + \imath (\hat{a} \cdot \vec{k}) u_k \right] d\mathbf{r} \quad (3.2)$$

This equation can now be broken into 2 terms: the first one involving $\vec{\nabla}_r u_k$, and the second one involving u_k . Again because of the orthogonality of Bloch function between the bands [12], the second term would be zero whenever $k = k'$, or when the momentum vector is not changed (nearly true in case of direct band gap material). Thus we can easily say that the second term would be very small as compared to first term. Considering this, the term involving $\vec{\nabla}_r u_k$ gives rise to *allowed term* of the matrix, while the term involving u_k is the *forbidden term*.

3.2.1.1 Allowed Term in Matrix Element H_{m0}

For this section, we will calculate the allowed term of the matrix element H_{m0} , involving $\vec{\nabla}_r u_k$. Thus the equation (3.2) reduces to,

$$\hbar_{k'k} = \frac{\imath \hbar e A}{2m} \int_{\Omega} u_{k'}^* \left[\hat{a} \cdot \vec{\nabla}_r u_k \right] d\mathbf{r} \quad (3.3)$$

The crystal momentum is defined as $\vec{p} = \hbar \vec{k} = -\imath \hbar \vec{\nabla}_r$, so we can write crystal momentum matrix as $\vec{p}_{k'k} \equiv -\imath \hbar \int_{\Omega} u_{k'}^* \vec{\nabla}_r u_k d\mathbf{r}$. This reduces the Hamiltonian matrix element (3.3) for allowed term to,

$$\hbar_{k'k} = \frac{eA}{2m} (\hat{a} \cdot \vec{p}_{k'k})$$

Using the above equation, we can reduce the transition probability for electron to make transition from state \mathbf{k} in valence band to state \mathbf{k}' in conduction band, defined in equation (2.17) as,

$$|A_{k'k}(t)|^2 = \frac{2\pi t}{\hbar} \left[\left(\frac{eA}{2m} \right)^2 (\hat{a} \cdot \vec{p}_{k'k})^2 \right] \delta(\xi_{k'} - \xi_k - \hbar\omega) \quad (3.4)$$

This is the transition probability of one primitive cell. To get the total transition probability for direct band to band transition, we will have to sum above equation (3.4) over all N allowed values of k , and that too over varying wavelength of the incoming photon, ω . Such a kind of calculation would become cumbersome, and would require computerized numerical techniques to solve them. Considering the limitation of this thesis, I have shown how to calculate the total probability, using the assumption that the incoming photon is monochromatic i.e. ω is constant. Once we have the transition probability for for monochromatic wave, we can integrate over all the values of ω , such as in the visible spectrum. We would also require certain other values, such as the volume occupied by each value of state \vec{k} , Fermi-Dirac distribution for getting the probability of valence shell being occupied, and conduction band being empty. These values are (proof excluded),

$$\text{Volume occupied by each value of } \tilde{k}: \quad \Omega_k = \frac{(2\pi)^3}{V} \quad (3.5)$$

$$\text{Fermi Dirac Distribution:} \quad f_0(E, T) = \frac{1}{1 + \exp[(E - E_f) / kT]} \quad (3.6)$$

E is the electron energy, and E_f is the Fermi Level in the material under consideration, k is the Boltzmann Constant, and T is the temperature of operation. Fermi Distribution (3.6) defines the probability of a state being occupied by an electron. Hence, the probability of state not being occupied is $1 - f_0(E, T)$. The total probability for an electron to transition between states, in a direct band gap material, can be calculated by integrating the transition probability (3.4) over the first Brillouin Zone, keeping in mind the Fermi Distribution for valence and conduction band. This total probability has to be multiplied by a factor of 2, to incorporate the effects of spin of an electron, during the absorption of photon. Hence, we can get the *total probability* $P_{k'k}$, and the *transition probability rate* $r_{k'k}$ ($= P_{k'k}/Vt$), as

$$P_{k'k} = \frac{2V}{(2\pi)^3} \int_{\Omega_k} |A_{k'k}(t)|^2 f_0(1 - f_0) d\vec{k} \quad (3.7)$$

$$r_{k'k} = \frac{2}{(2\pi)^3} \int_{\Omega_k} \frac{|A_{k'k}(t)|^2}{t} f_0(1 - f_0) d\vec{k} \quad (3.8)$$

Using the transition rate $A_{k'k}$, calculated in (3.4), we can write the transition probability rate $r_{k'k}$ as,

$$r_{k'k} = \frac{e^2 A^2}{8 \pi^2 \hbar m^2} \int_{\Omega_k} (\hat{a} \cdot \vec{p}_{k'k})^2 \delta(\xi_{k'} - \xi_k - \hbar \omega) f_0 (1 - f_0) d\vec{k} \quad (3.9)$$

Going ahead with the parabolic band assumption, from figure 3.1, we can write

$$\begin{aligned} \xi_{k'} - \xi_k &= \xi_g + \frac{\hbar^2 k'^2}{2 m_e} + \frac{\hbar^2 k^2}{2 m_h} \\ &\approx \xi_g + \frac{\hbar^2 k^2}{2 m_r} \quad (\text{assuming } k' \cong k) \end{aligned}$$

ξ_g is the energy band gap for the material, m_e is the mass of the electron with wavevector k' , and m_h is the mass of the hole with wavevector k . m_r is the reduced mass for the electron and the hole. In the equation defining the transition probability rate (3.9), we can see that compared with the Dirac-Delta term, all other terms inside the integral vary very slowly with the variation of k . Thus we can easily take these terms out of the integral, without any loss. We define a dimensionless term *oscillator strength* [15] $O_s \equiv \frac{2(\hat{a} \cdot \vec{p}_{k'k})^2}{m \hbar \omega}$. Also we know, that $d\vec{k} = 4\pi k^2 dk$. Thus, the equation (3.9), can be evaluated as,

$$r_{k'k} = \frac{e^2 A^2}{8 \pi^2 \hbar m^2} f_0 (1 - f_0) \left(\frac{O_s \hbar m \omega}{2} \right) \int_{\Omega_k} \delta \left(\xi_g + \frac{\hbar^2 k^2}{2 m_r} - \hbar \omega \right) 4\pi k^2 dk \quad (3.10)$$

The delta function has a property, such that

$$\int_{-\infty}^{\infty} f(x) \delta(x - a) dx = f(a)$$

Using the above property in equation (3.10), we get the transition probability rate as,

$$r_{k'k} = \left(\frac{e^2 \sqrt{m}}{8\pi\hbar^3} \right) \left(\frac{2m_r}{m} \right)^{1.5} A^2 \omega O_s f_0 (1 - f_0) \sqrt{\hbar\omega - \xi_g} \quad (3.11)$$

Absorption Coefficient is defined as the transition rate per unit quantum flux (quantum flux is defined as the number of incident photons per unit area in unit time). Quantum flux can be calculated from the average value of Poynting Vector \mathbf{S} per unit wavelength energy. The various relations are given below:

$$\text{Quantum Flux : } \Phi = \frac{\langle \vec{S} \rangle}{\hbar\omega}$$

$$\text{Poynting Vector : } \vec{S} = \vec{E} \times \vec{H}$$

$$\text{Electric Field : } \vec{E} = A\omega \hat{a} \sin(\vec{q} \cdot \vec{r} - \omega t)$$

$$\text{Magnetic Field : } \mu \vec{H} = -A (\vec{q} \times \hat{a}) \sin(\vec{q} \cdot \vec{r} - \omega t)$$

$$\text{Average Poynting Vector : } \langle \vec{S} \rangle = \frac{1}{2} |q| \frac{\omega A^2}{\mu} = \frac{1}{2} \eta \epsilon_0 c \omega^2 A^2$$

Using above relations, we can solve for Absorption Coefficient, α ($= r/\Phi$), as

$$\alpha_{allowed} = \left(\frac{e^2 \sqrt{m}}{4\pi\epsilon_0 c \hbar^2} \right) \left(\frac{2m_r}{m} \right)^{1.5} \left(\frac{O_s}{\eta} \right) f_0 (1 - f_0) \sqrt{\hbar\omega - \xi_g} \quad (3.12)$$

3.2.1.2 Forbidden Term in Matrix Element H_{m0}

In this section, let us consider the forbidden term, containing u_k , in the matrix element H_{m0} .

Thus, the matrix element reduces to,

$$\hbar_{k'k} = -\frac{\hbar eA}{2m} \int_{\Omega} u_{k'}^* u_k d\mathbf{r} \quad (3.13)$$

Using this equation with the transition probability (2.17), the forbidden transition probability for electron transition from state \vec{k} in valence band to state \vec{k}' in conduction band, is given by,

$$|A_{k'k}(t)|^2 = \left(\frac{2\pi t}{\hbar} \right) \left(\frac{e\hbar A}{2m} \right) |\hat{a} \cdot \vec{k}|^2 O'_s \delta(\xi_{k'} - \xi_k - \hbar\omega) \quad (3.14)$$

The *forbidden oscillator strength*, defined as $O'_s = |\int_{\Omega} u_{k'}^* u_k d\mathbf{r}|$. For all values of $\vec{k} \neq \vec{k}'$, $0 < O'_s \ll 1$. To evaluate the forbidden total transition probability, and the forbidden

transition rate, integrate equation (3.14) over the first Brillouin Zone, keeping in mind the Fermi distribution. For ease of calculation, we take the average value of $|\hat{a} \cdot \vec{k}|$ as $k/\sqrt{3}$ (averaging in 3 directions). Thus the forbidden transition rate, and the forbidden absorption coefficient are,

$$r_{k'k} = \left(\frac{e^2 \sqrt{m}}{12\pi\hbar^4} \right) \left(\frac{2m_r}{m} \right)^{2.5} A^2 \omega O'_s f_0 (1 - f_0) \sqrt{(\hbar\omega - \xi_g)^3} \quad (3.15)$$

$$\alpha_{forbidden} = \left(\frac{e^2 \sqrt{m}}{6\pi\epsilon_0 c\hbar^2} \right) \left(\frac{2m_r}{m} \right)^{2.5} \left(\frac{O'_s}{\eta} \right) f_0 (1 - f_0) \frac{\sqrt{(\hbar\omega - \xi_g)^3}}{\hbar\omega} \quad (3.16)$$

3.2.2 Indirect Band Gap Transition

In case of indirect transition, absorption or emission of a phonon is necessary, to conserve the wavevector. Simultaneous absorption of a photon and phonon being high-order process, and hence have lesser probability, but the additional degree of freedom introduced by phonon energy $\hbar\omega_s$ makes the transition probability increase as transitions to many more states are possible. Analysis of indirect transition can be done by means of direct transition from state 0 to a virtual state I_c with simultaneous absorption/emission of a phonon to scatter electron from I_c to m . The other way of analysis can be done by considering emission of a phonon to scatter from 0 to a virtual state I_v with a simultaneous direct transition from I_v to m . This is shown in figure 3.2

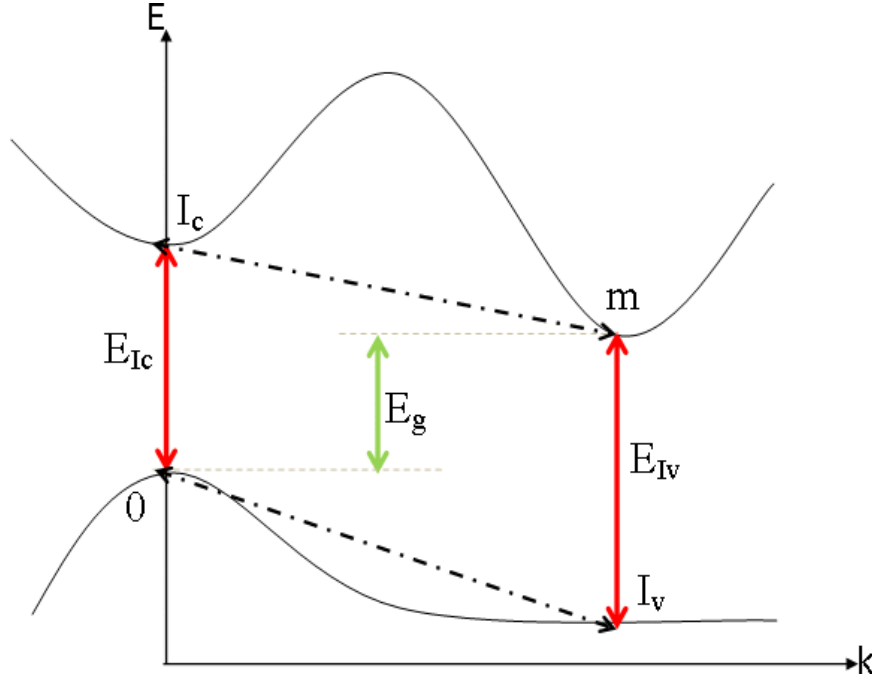


Figure 3.2: E-k diagram for photon induced indirect-gap electron transition. Shows two possible mechanisms for electron to transit between states 0 and m , via intermediate state I_v or I_c

The derivation of transition rate and associated absorption coefficient for indirect transition is beyond the scope of this thesis. They can be analyzed by second-order perturbation theory, and can be understood from [16]. I here just give the results. Considering the virtual state in conduction band i.e. transition occurring through intermediate state as I_c , we get the allowed absorption coefficient as,

$$\alpha_{c,allowed} = \left(\frac{m_h^{1.5} e^2}{32 \pi \epsilon_0 c m \hbar \sqrt{m_e}} \right) \left(\frac{g_c O_s^c \omega_s}{l_c \omega \eta} \right) \left(\frac{\xi_{Ic}}{kT} \right) \left(\frac{\hbar \omega \pm \hbar \omega_s - \xi_g}{\xi_{Ic} - \hbar \omega} \right)^2 \frac{\pm 1}{\exp(\pm \hbar \omega_s / kT) - 1}$$

TRANSITION TYPE	DEPENDENCE ON $(\hbar\omega - \xi_g)$
Direct Allowed Transition	Varies as $(\hbar\omega - \xi_g)^{1/2}$
Direct Forbidden Transition	Varies as $(\hbar\omega - \xi_g)^{3/2}$
Indirect Allowed Transition	Varies as $(\hbar\omega - \xi_g)^2$
Indirect Forbidden Transition	Varies as $(\hbar\omega - \xi_g)^3$

Table 3.1: Band-to-Band Transition

The + and - signs are for the absorption and emission of phonons respectively, with phonon frequency ω_s . g_c is the number of conduction band minima, and O_s^c is the oscillator strength for conduction band transition, and l_c is the mean free path for electron scattering in the conduction band. Taking virtual state in valence band, we get the allowed absorption coefficient as

$$\alpha_{v,allowed} = \left(\frac{e^2 m_e^{1.5}}{32 \pi \epsilon_0 c m \hbar \sqrt{m_h}} \right) \left(\frac{g_c O_s^v \omega_s}{l_v \omega \eta} \right) \left(\frac{\xi_{lv}}{kT} \right) \left(\frac{\hbar\omega \pm \hbar\omega_s - \xi_g}{\xi_{lv} - \hbar\omega} \right)^2 \frac{\pm 1}{\exp(\pm \hbar\omega_s / kT) - 1}$$

The + and - signs are for the absorption and emission of phonons respectively. O_s^v is the oscillator strength for valence band transition, and l_v is the mean free path for electron scattering in the valence band. Thus the total allowed absorption coefficient is

$$\alpha_{allowed} = \alpha_c(+\omega_s) + \alpha_c(-\omega_s) + \alpha_v(+\omega_s) + \alpha_v(-\omega_s) \quad (3.17)$$

We can also calculate the forbidden transition absorption coefficient, which are not a part of this thesis, but can read in detail in [16]. Thus from above equations and equations for direct gap transitions, we can draw the following conclusion shown in Table 3.1.

3.3 Exciton Level Electron Transition

Exciton, by definition, is an electron-hole pair bounded by Coloumbic attraction between the pair. These exist at very low thermal energy, as the thermal energy ($\cong kT$) at room temperatures is enough to dissociate them. Their existence at room temperatures is possible in quantum structures at room temperatures due to localization of electron in these quantum confined structures. Excitonic level absorption leads to absorption spectra just below the fundamental absorption edge, as shown in figure 3.3.

Situation in figure 3.3 is analogous to a hydrogen model. For the n binding energies of exciton, it can move throughout the crystal with dispersion relation given by (in eV),

$$\begin{aligned}\xi_{xn} &= 13.6 \left(\frac{1}{n \epsilon_r} \right)^2 \left(\frac{m_r}{m} \right) \\ \xi_{xn}(\vec{k}) &= \xi_{xn} + \left(\frac{\hbar^2 k^2}{2M} \right)\end{aligned}\tag{3.18}$$

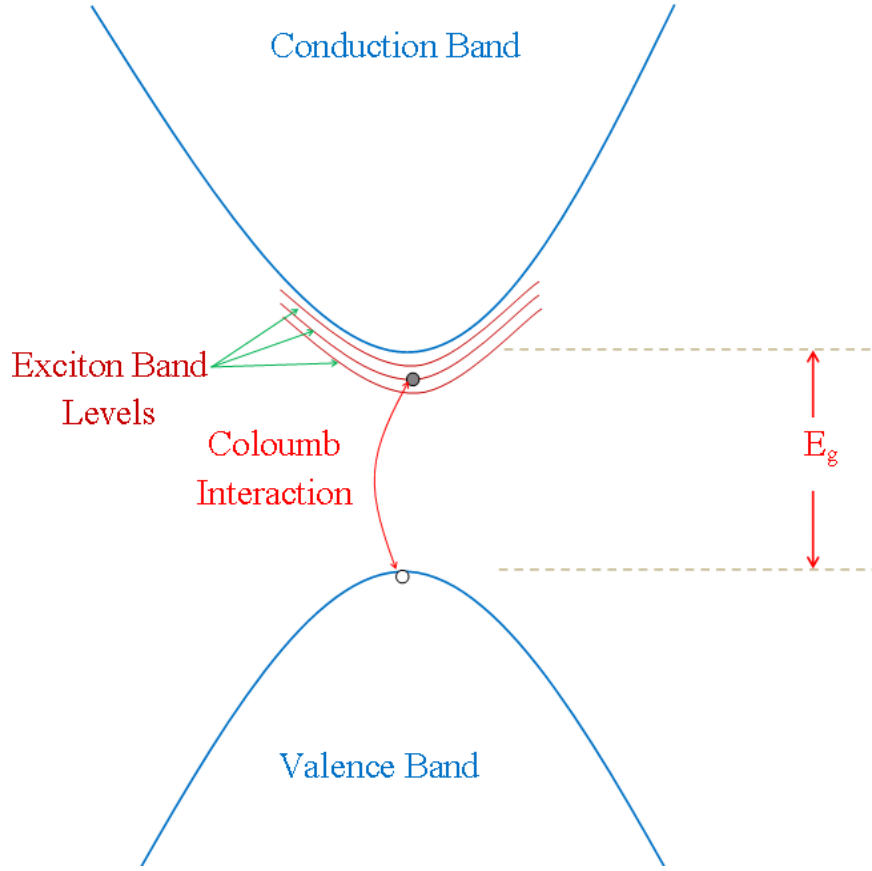


Figure 3.3: Variation of band structure due to exciton formation. Shows the coulombic attraction between the electron-hole pair

m_r is the reduced mass for electron and hole, n is the number of exciton levels, ϵ_r is the dielectric constant of the material, and M is the combined effective mass of electron-hole pair, given by $M = m_e + m_h$. This exciton model is very similar to the direct band gap absorption discussed in section 3.2.1, and thus using the results for direct band gap transition, we can write the exciton absorption coefficient as,

$$\alpha_{ex,allowed} = \left(\frac{e^2 \sqrt{m}}{4\pi\epsilon_0 c \hbar^2} \right) \left(\frac{2m_r^*}{m} \right)^{1.5} \left(\frac{O_s}{\eta} \right) f_0 (1 - f_0) \sqrt{\hbar\omega - \xi_g - \xi_x n} \quad (3.19)$$

m_r^* is the reduced mass of the combined system for exciton and the hole, given as,

$$\frac{1}{m_r^*} = \frac{1}{M} + \frac{1}{m_h}$$

3.4 DOS, and Fermi Energy Dependence

The absorption coefficient for all cases discussed till now, direct band gap transition 3.2.1, indirect band gap transition 4.2.2, or the exciton level transition 3.3, we have the fermi energy dependence in the form of the Fermi Distribution f_0 . We define the Fermi Distribution as,

$$f_0 = \frac{1}{1 + \exp(\xi - \xi_f/kT)}$$

This is a simple equation, where the effect of doping profile is considered in the definition of fermi level energy ξ_f . Or we can put it this way, that if there is no doping (or very low

doping profile), above equation can be used to calculate the Fermi - Dirac distribution. We make the calculation with respect to $E_f \pm 4kT$, as $4kT$ determines the energy window for which the Fermi - Dirac distribution rapidly decays to zero (+), or rapidly approaches one (-).

In cases of a very heavy doping profile ($> 10^{20} \text{ cm}^{-3}$), the above equation cannot be used. For illustration, let us assume we are considering a highly n doped material. In such kind of material, the Fermi level ξ_f will be inside the conduction band. So now we can comfortably say that all the states in valence band, and all the states in conduction band from bottom of conduction band to $\xi_f - 4kT$ will be occupied. Hence, now the energy required by the photon to transit an electron from a filled state in valence band to an empty state in conduction band will be greater than the band gap of the material. This is shown in figure 3.4.

From the above figure 3.4, the energy required by a photon for electron transition is given by

$$\hbar \omega = \xi_g + \frac{\hbar^2 k^2}{2m_r} \quad (3.20)$$

m_r is the reduced effective mass for the electron and hole. Thus, we can see that the fundamental absorption edge has moved due to doping. We can use the above equation

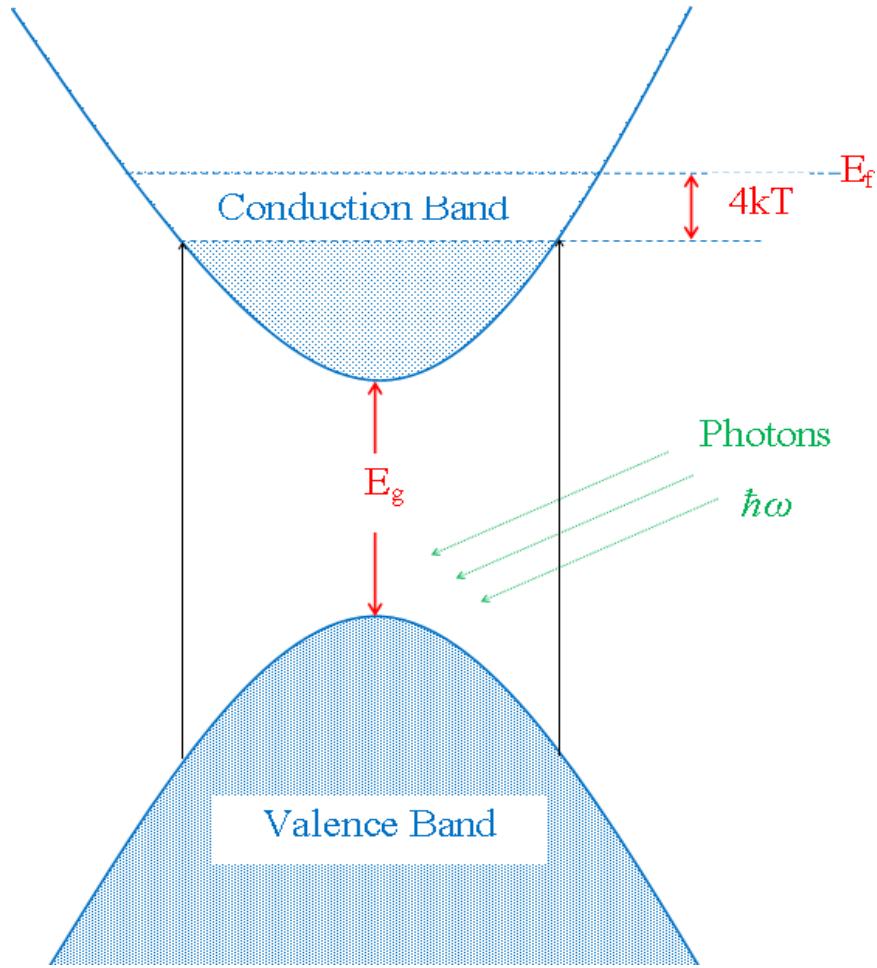


Figure 3.4: Fundamental Absorption Edge in a heavy n-doped (n^+) doped material. Shaded region depicts fully filled energy levels. The fermi level ξ_f lies in the conduction band.

to modify the results for direct band gap absorption coefficient for doped materials. This effect is called the *Burstein-Moss shift*. We will also have to take into account the change in the Fermi distribution.

3.5 Photoluminescence (PL)

The photoluminescence intensity spectrum $\tau(\xi)$ can be related to the absorption coefficient $\alpha(\xi)$, using the van Roosbroeck - Shockley equation [17, 18] using the principal of detailed balance, as

$$\tau(\xi) \propto \frac{\eta^2 \xi^2 \alpha(\xi)}{\exp\left[\left(\frac{\xi}{kT_c}\right) - 1\right]} \quad (3.21)$$

ξ is the energy of the photon ($= \hbar\omega$), k is the Boltzmann constant, η is the refractive index of the material, and T_c is the actual carrier temperature. The close agreement of the spontaneous emission spectrum, equation (3.21), with the experimentally observed PL Spectra, will demonstrate the correctness of shape and value for the measured/calculated absorption coefficient, $\alpha(\xi)$.

Chapter 4

RESULTS AND DISCUSSION FOR ABSORPTION COEFFICIENT AND PHOTOLUMINESCENCE

This chapter describes the plots for the absorption coefficients calculated in chapter 3. I have assumed values for various parameters, and have discussed them as we go along. These parameters have been calculated according to work done in [19, 20, 21]. For ease of calculation and reasons explained ahead, the plots here are only for allowed terms, having neglected any influence of forbidden transition coefficients.

The results have been discussed for silicon nanostructures, which show band gap variation

depending upon the confinement which is directly related to the size and geometry of the structure. We consider silicon quantum dots (QDs), which have known to show direct band gap transition [20, 22], for diameters for the QDs in confinement region, and have shown in-direct band gap behavior [23, 24] for other diameters. The diameter of the QD defines the band gap energy. The differences between the data on energy band gaps are possibly associated with the dependence of the electronic properties of the QDs on the dot shape and the surrounding layers, and hence fabrication techniques.

Before we plot the values for absorption coefficients, we need to define any other dependence on wavelength (such as refractive index η , etc.).

4.1 Refractive Index

From first view of equations defining the absorption coefficients (equations 3.12, 3.16, 3.17, 3.19), one can see that the absorption coefficient depends only on the frequency (or the wavelength) of the incoming photon, and is independent of the spatial dependence of the nanostructure. But this might not be true, and the hidden dependence can be seen in the refractive index η of the material. The complex refractive index of the nanostructure can be defined as (η_r is the real part, and η_i is the imaginary part),

$$\eta = \eta_r - i\eta_i \quad (4.1)$$

λ is the wavelength of the light in vacuum. For our calculations, since we are concentrating in the visible spectrum, the extinction coefficient is negligible as it diminishes for frequency greater than 400nm [9]. Hence, we want the variation for the real part of the refractive index with the wavelength of the light, or the incoming photon to be precise. The data taken from [9], has been curve fitted using the Herzberger formula [25] used as a variation of Sellmeier formula[26], as

$$\eta_r = \beta_a + \frac{\beta_b}{\lambda^2 - 0.0028}$$

β_a and β_b are material constants, and are required to be calculated experimentally. λ is the wavelength of the light in vacuum (in μm). The constant 0.0028 is an arbitrary choice, independent of material. After curve fitting from the experimental data [9], the constants are evaluated as $\beta_a = 3.2346$ and $\beta_b = 0.3698$. The Herzberger's formula for refractive index of Silicon then is,

$$\eta_r = 3.2346 + \frac{0.3698}{\lambda^2 - 0.0028} \quad (4.2)$$

We are using this relationship, equation (4.2), for calculating the absorption coefficient in silicon QDs. One thing that we might be concerned with is that this might not be a true relationship in QDs, as the data has been generated for bulk silicon. Due to paucity of time, and no data availability for silicon QDs, this is the relation we have to work with. This variation of refractive index is shown in figure 4.1.

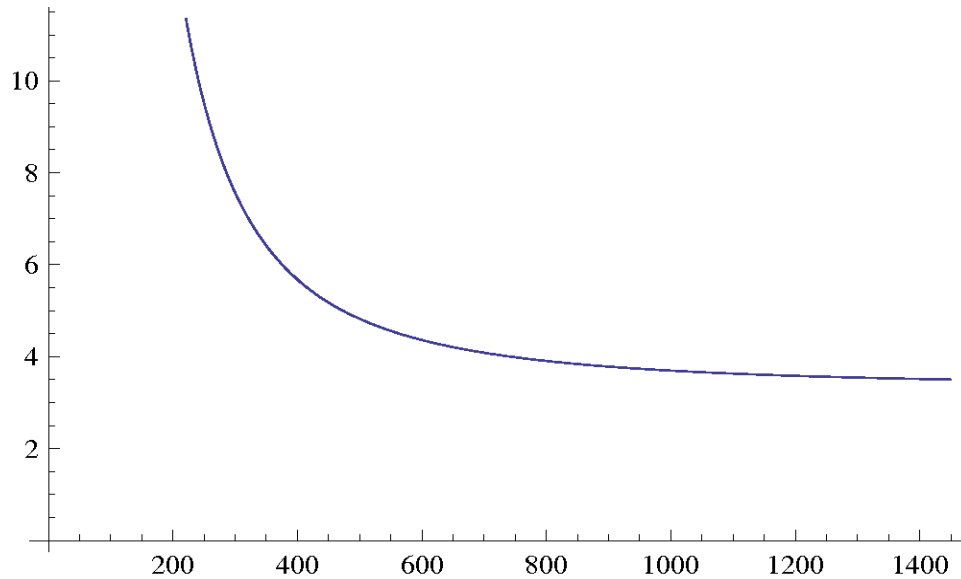


Figure 4.1: Variation of Refractive Index n (y-axis) with the wavelength λ (μm) of incoming photon

4.2 Intra-band Absorption of Photons

We will take the following assumption for the calculations of absorption coefficient for direct/indirect/exciton electron transition.

1. **Effective mass of electron, and hole:** For the mass of electron and hole involved in the transition from valence band to conduction band, we take the effective conduction masses. Effective mass of electron is $m_e = 0.26 m_0$, and effective mass of hole is $m_h = 0.36 m_0$, where m_0 is the rest mass of electron.,

2. **Oscillator Strength O_s :** Due to paucity of information, and knowledge, I could not dwell more into the study of Oscillator Strength. This study involves a good knowledge of Quantum Field Theory, which is beyond the scope of this thesis. This is one area where more focus needs to be devoted. I have taken the Oscillator strength for all possible cases as one. This is a point of contention for quantum confined structures, though this might hold true for these structures, as has been shown [15].

3. **Fermi Distribution f_0 :** For the ease of calculations, the material is take as undoped. We also assume the ideal condition that all states in valence band are filled, and all the states in conduction band are empty. Thus, $f_0 = 0.5 = 1 - f_0$.

4.2.1 Direct Band Gap Transition

The absorption coefficients for direct band gap transitions calculated in sections 3.2.1.1 and 3.2.1.2 were

$$\alpha_{allowed} = \left(\frac{e^2 \sqrt{m}}{4\pi\epsilon_0 c \hbar^2} \right) \left(\frac{2m_r}{m} \right)^{1.5} \left(\frac{O_s}{\eta} \right) f_0 (1 - f_0) \sqrt{\hbar\omega - \xi_g} \quad (4.3)$$

$$\alpha_{forbidden} = \left(\frac{e^2 \sqrt{m}}{6\pi\epsilon_0 c \hbar^2} \right) \left(\frac{2m_r}{m} \right)^{2.5} \left(\frac{O'_s}{\eta} \right) f_0 (1 - f_0) \frac{\sqrt{(\hbar\omega - \xi_g)^3}}{\hbar\omega} \quad (4.4)$$

The first bracket $\left(= \frac{e^2 \sqrt{m}}{6\pi\epsilon_0 c \hbar^2} \right)$ are all constants, and thus can be evaluated easily. Using the Fermi distribution defined above, the allowed and forbidden term for absorption coefficient can be written as

$$\alpha_{allowed} = 2.7 \times 10^{-5} \left(\frac{2m_r}{m} \right)^{1.5} \left(\frac{O_s}{\eta} \right) f_0 (1 - f_0) \sqrt{\hbar\omega - \xi_g} \quad (4.5)$$

$$\alpha_{forbidden} = 1.8 \times 10^{-5} \left(\frac{2m_r}{m} \right)^{2.5} \left(\frac{O'_s}{\eta} \right) f_0 (1 - f_0) \frac{\sqrt{(\hbar\omega - \xi_g)^3}}{\hbar\omega} \quad (4.6)$$

If we compare the above two equations, we can note that the allowed term for transition is much greater than the forbidden term for transition. Thus we can easily neglect the forbidden term. This is shown in the plot 4.2, where the probability of forbidden transition to allowed transition is 1 : 9, which technically is very high for forbidden term. Such a high value has been taken to show that at even this high value, the forbidden term's value is very small as compared to the allowed transition term. The plot has been done for a energy band gap of 1.69 eV [20] for a QD structure of 5 nm diameter, oscillator strengths of $O_s = O'_s$,

refractive index of silicon as described above. Thus, for our further discussion, we will ignore the contribution due to the forbidden term without any loss.

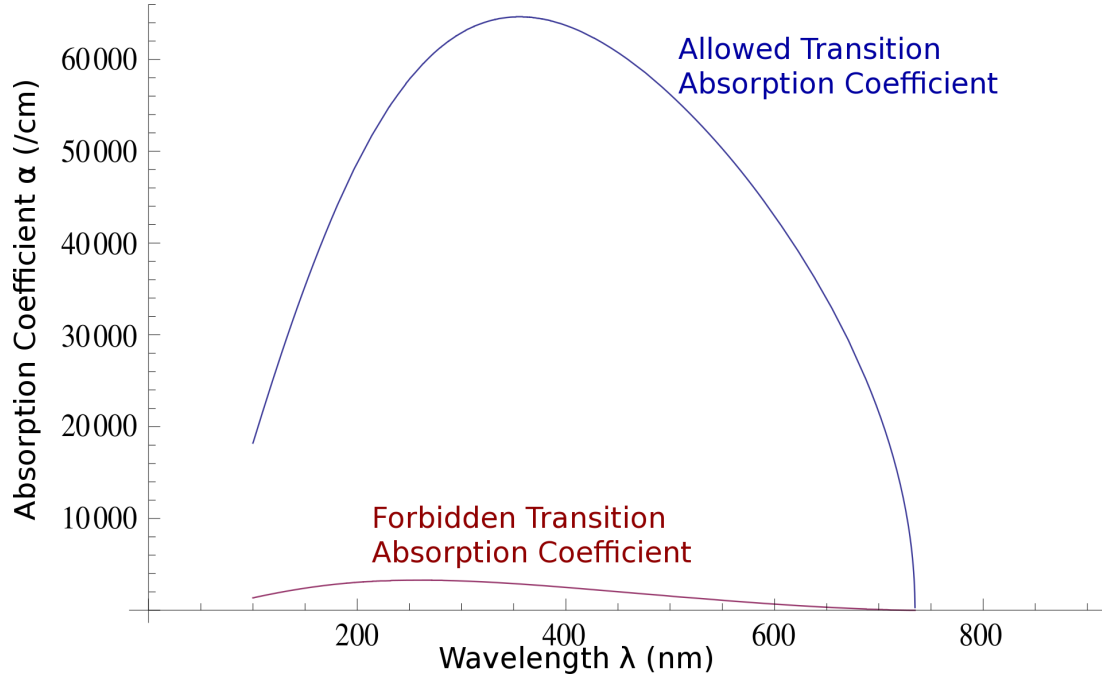


Figure 4.2: Comparison of absorption coefficient α , for allowed and forbidden transition for a 9:1 probability

Figure 4.3 has been plotted for varying band gap ξ_g , which will happen for a array cluster of QDs of varying sizes, as discussed in chapter 1. The figure shows the band gap varying from 1.12 eV (the bulk silicon limit) to 3.65 eV (maximum band gap for smallest possible practically fabricated silicon QD).

We first concentrate on absorption coefficient curve for a single band gap as shown in figure 4.2. We observe the onset of optical absorption for energies of photon $\xi > 1.687 \text{ eV}$ ($= 734.742 \text{ nm}$), the band gap assumed for nanostructure silicon here. The absorption co-

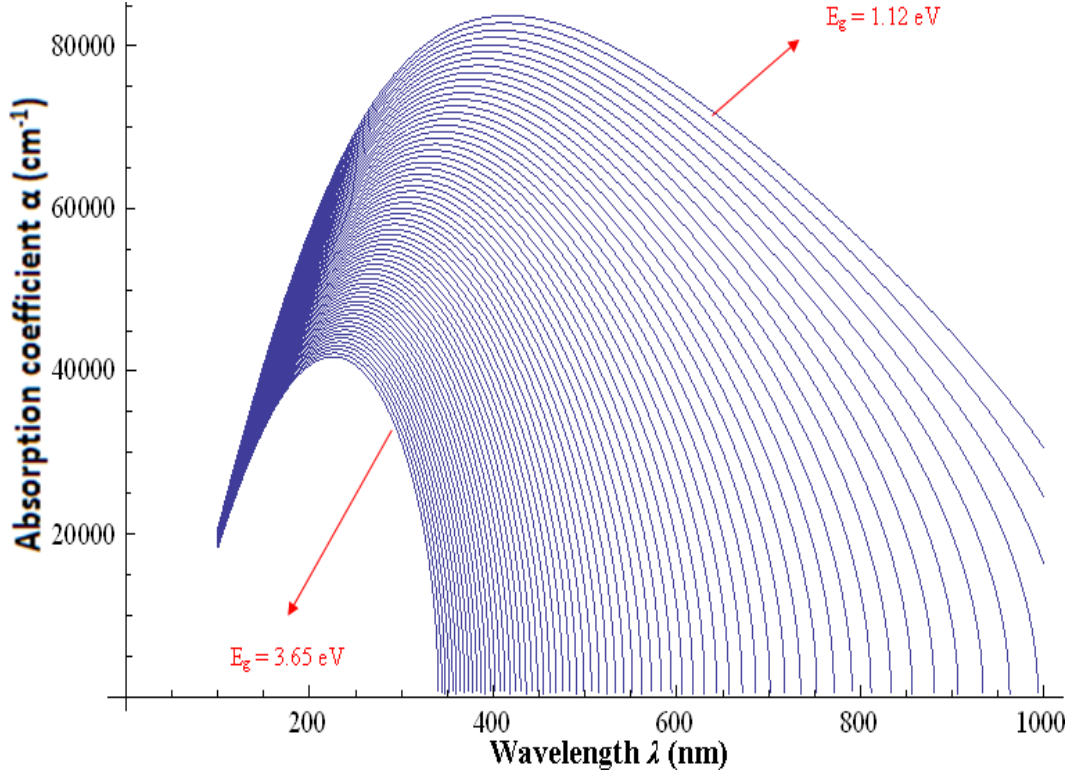


Figure 4.3: Variation of Absorption coefficient α for direct band gap transition, for photons with varying incoming wavelength λ , and for a array of Silicon QDs of varying band gap ξ_g , for dots under quantum confinement

efficient, α , quickly increases from 10000 cm^{-1} to 64000 cm^{-1} , and reaches a maximum of 64638.2 cm^{-1} at photon energy of $\xi = 3.49\text{ eV}$ ($= 355.532\text{ nm}$). Similarly, if we do analysis for band gap of $\xi_g = 1.82\text{ eV}$, we get the onset at $\xi > 1.818\text{ eV}$ ($= 682.261\text{ nm}$), and it reaches a maximum of 62344.5 cm^{-1} at photon energy of $\xi = 3.61\text{ eV}$ ($= 343.402\text{ nm}$). Smith A. et al. [27], have performed time resolved PL measurements on silicon nanoparticles (1 nm) and have reported direct band to band transition with emission in the wavelength range of $380\text{-}450\text{ nm}$. Thus, this result matches very well with our calculated result for absorption spectra peak. Our theoretical plots are further proved right as these authors

also note that polysilane displays strong absorption from 280 – 350 *nm*.

One point of contention here is that we should have observed just resonant peaks when we consider nanostructures, such as these Silicon QDs, as was proved theoretically in the transition probability 2.17. In the equation for transition probability, we consider the conduction band edge ξ_c to be discrete, instead of continuous. This is true in case of silicon QDs, which will show discreteness in levels or states of conduction band (and of valence band too) due to confinement in all the three dimensions. But when we simulate for the results, we have taken continuous bands for ease of calculation, and we assume that the transition is taking place from the highest level in valence band to the lowest level in conduction band. Also we are ignoring the Pauli's Exclusion Principle for each possible state in conduction band.

The decrease of absorption coefficient for low values of wavelength is related to significant increase in refractive index with decreasing wavelengths which is questionable in silicon nanostructures. Schmitt-Rink et al. [28] show a peak in absorption coefficient α with a bandwidth (0.5 *meV*) for GaAs quantum dots. These authors claim that quantum dots have a substantial advantage in enhancing optical absorption, and similar has been observed in our plots.

Figure 4.3 depicts the effect of various silicon quantum dots in a solar cell of QD array. Due to quantum confinement, the energy band gap of QD increases with decreasing diameter. Here QDs in the range of 2nm to 10nm have been considered, which exhibit quantum

confinement. As seen here, the onset of absorption shifts to left with increasing bandgap ξ_g as expected, and the maximum decreases and shifts to the left. This peak shows a blue shift as the band gap energy increases from 1.12eV towards 3.65eV. The shifting of the maximum with lowering wavelengths is also an expected result since the dependence of absorption coefficient on refractive index is more pronounced at lower wavelengths and the factor $\sqrt{\hbar\omega - \xi_g}$ decreases with increasing ξ_g .

4.2.2 Indirect Band Gap Transition

For indirect band gap transition, we only consider the allowed terms. We make use of the total allowed transition absorption coefficient defined in equation 3.17. There are a lot of variables that we need to define or assume for plotting this kind of transition. One thing to keep in mind is that strong quantum confinement in silicon increases the probability of combination through radiation via the direct-band gap transition, and hence reduces the electron-phonon interaction [24], effectively reducing the indirect band gap transition. For QDs bigger in diameter than 8nm, exhibit indirect band gap [24, 21], and do not exhibit a strong confinement in all directions.

4.2.3 Exciton Level Electron Transition

Referring to figure 3.3 again, due to localization of electrons in these excitonic states, the effect of such kind of absorption will be very significant in nanostructures, specially QDs. We plot the n -binding energies for excitonic levels with $n = 5$ in figure 4.4, defined by following equation.

$$\xi_{xn} = 13.6 \left(\frac{1}{n \epsilon_r} \right)^2 \left(\frac{m_r}{m} \right)$$

The electron, however, will only be present in any one of these n ($= 5$ in this case) possible excitonic states. Taking the other values similar to those in case of direct gap absorption 4.2.1, figure 4.5 and 4.6 shows the absorption coefficient for excitonic behavior for varying band gap and one particular band gap respectively.

The absorption coefficient peak is higher for excitons; this was expected as we have localization of electrons in these excitonic states, and thus higher transition probability. In figure 4.5, we observe a broad spectrum for absorption, instead of the expected resonance curve. This is because we consider only one possible excitonic level for all calculations while plotting the curve in figure 4.5. The resonance of peaks in absorption is seen in figure 4.6, where we have plotted for all possible excitonic levels shown in figure 4.4. This

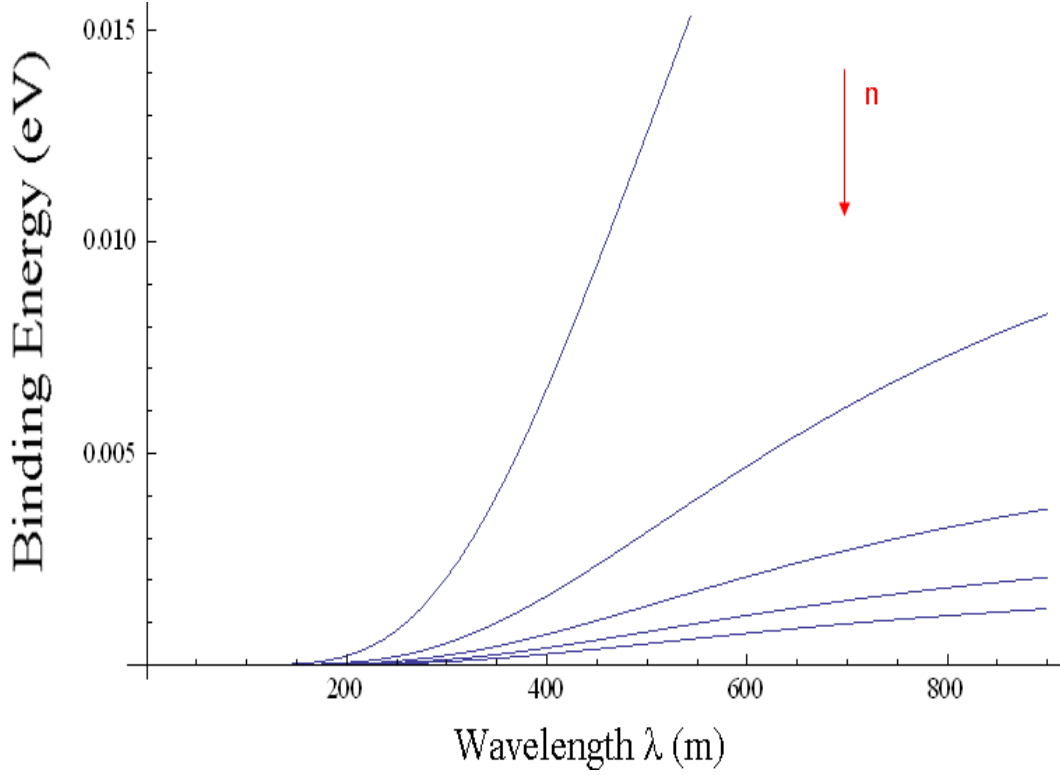


Figure 4.4: $n = 5$ exciton states binding energy variation with wavelength

is done for a band gap of $\xi_g = 1.69 \text{ eV}$. The peaks in the figure 4.6 occur at 354.665nm, 355.313nm, 355.434nm, 355.477nm, and 355.497nm respectively.

4.3 Photoluminescence (PL)

The PL spectra is calculated using equation (3.21) in section 3.21. This PL spectra was calculated using the exciton absorption coefficient of figure 4.6 for $\xi_g = 1.69 \text{ eV}$.

Though all these 5 possible excitonic states were considered in generating the plot, in

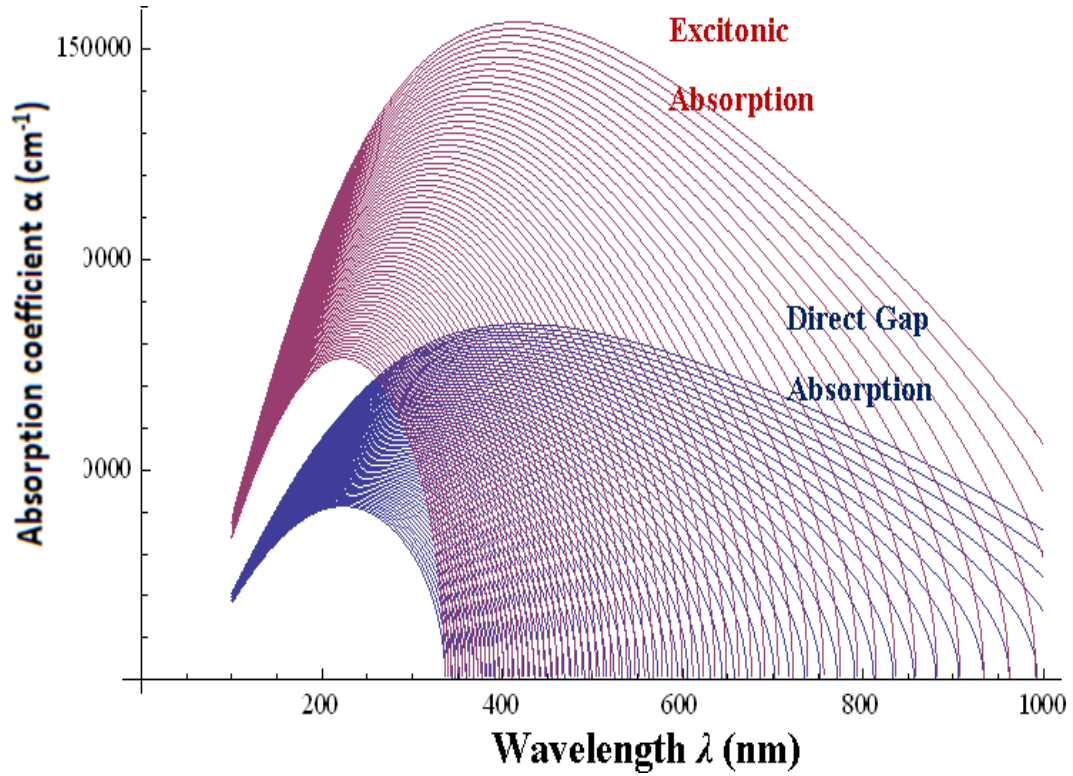


Figure 4.5: Comparative plots for exciton and direct gap absorption, keeping all other parameters same. The band gap varies from 1.12 eV to 3.65 eV

reality, an electron can occupy only one of these states. The highlighted curve shows the expected PL spectra, as an electron during transition will not occupy all the n possible states. Also in a particular state, it will try and be near the peak of that particular state, as it makes electron closer to the conduction band minima. The plot is shown in figure 4.7, and if we compare the results with the experimental results from [29], we see a very close match between the results, and thus we can say that our calculated PL is a close match with that of experimental data.

Our theoretical results for PL are in conjunction with the experimental results. These results

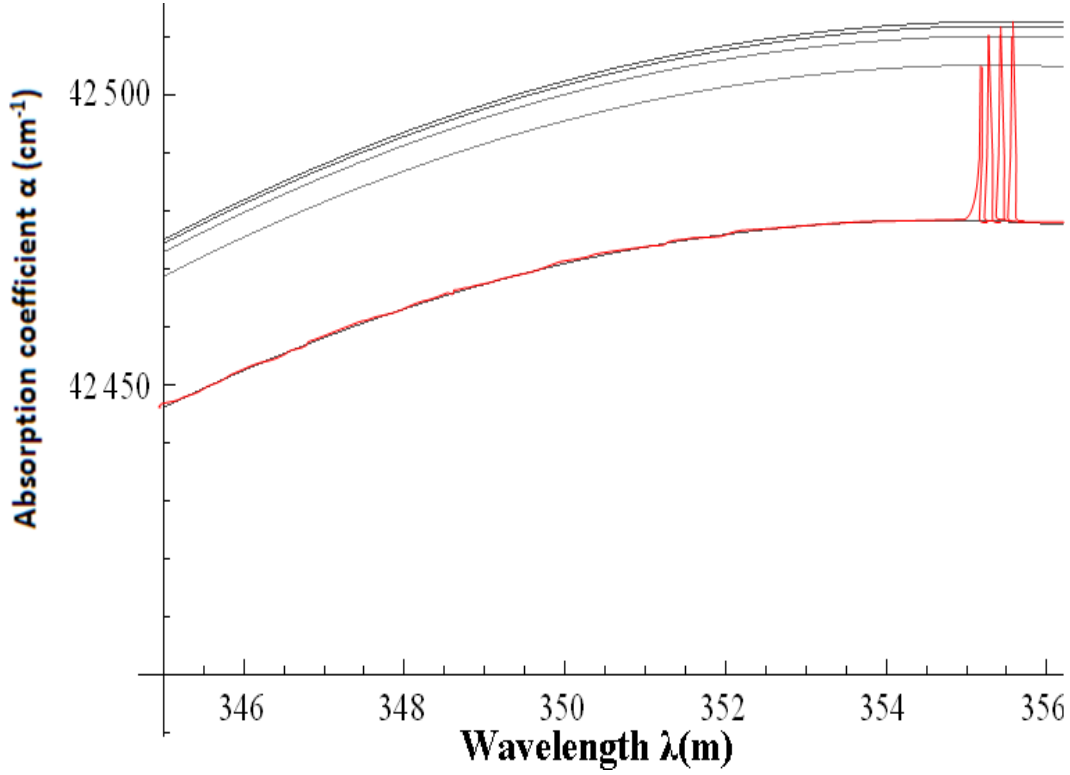


Figure 4.6: Exciton absorption curve showing the resonance peaks for $n = 5$ possible states, for $\xi_g = 1.69 \text{ eV}$

have been plotted from our derived equation for absorption coefficient, and thus we can say that our results shown in figure 4.3 and 4.5 should be fairly consistent. Thus all in all we can say that is very good correlation between the existing results and the theoretical results proposed here.

The radiative recombination times for Silicon QDs were calculated in [30], and were compared against the experimentally observed PL experimental lifetime [31]. The observed PL experimental lifetime for Silicon QDs showed that lifetime sharply decreases with the size. This experimental time is approximately 30 times smaller than the calculated recombina-

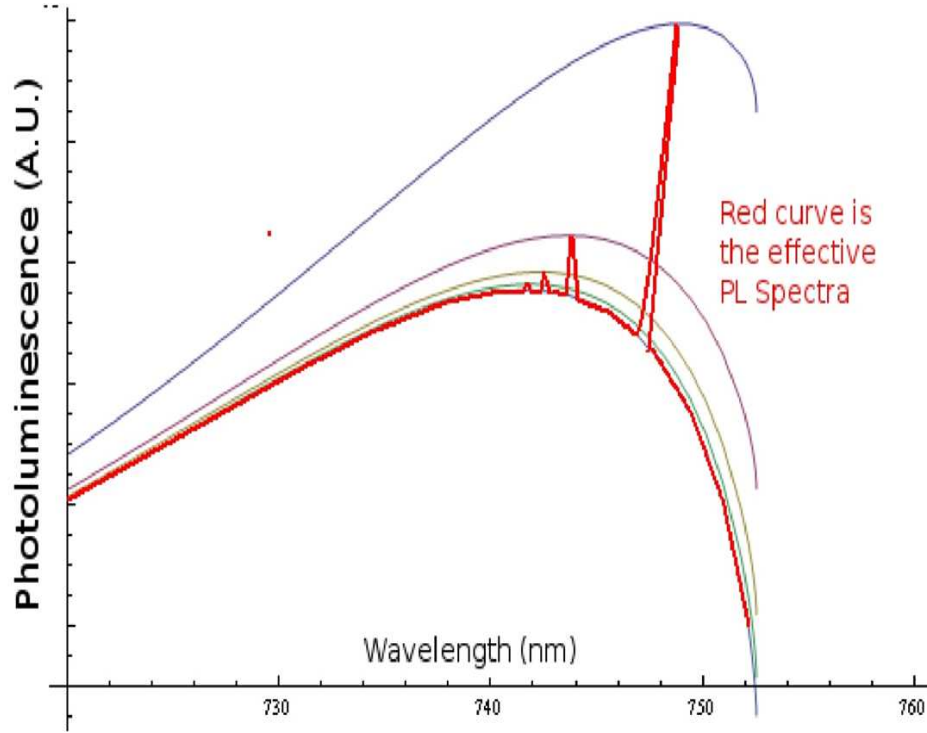


Figure 4.7: The highlighted curve shows the actual PL spectra expected, as the electron while transiting will not occupy all the states

tion time [30]. This discrepancy in results is attributed to the uncertainties in the calculation of various other factors (such as refractive index η , etc.). But this does not negate the possibility of other non-radiative recombination mechanisms. The calculated recombination times are of the order of 10^3 ps, while the calculated times are of the order of 10^2 ps [30].

The absorption coefficient curve for single band gap material, taken as Si for continuity and comparison with band gap energy of 1.12 eV , is shown in plot 4.8.

Comparing the absorption coefficient curves for direct gap quantum dots of silicon (figure 4.3) and bulk silicon solar cell (figure 4.8), we can see that for bulk silicon solar cell, the

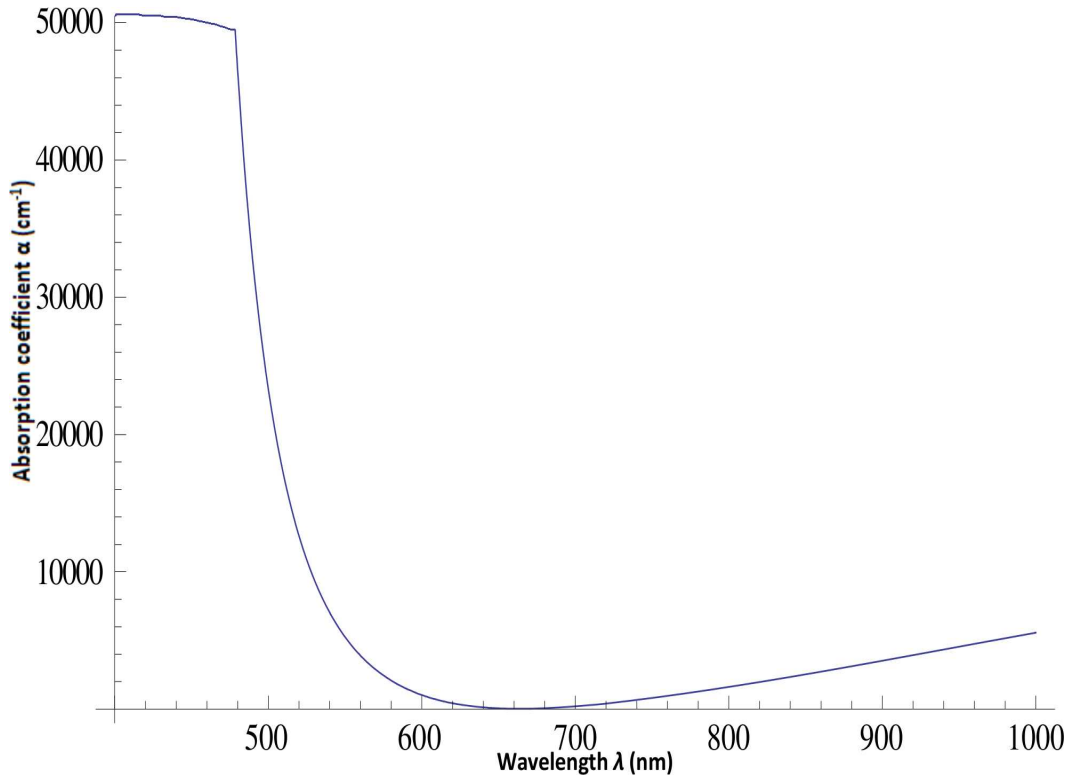


Figure 4.8: Absorption Coefficient Curve for Silicon Bulk Solar Cells of 1st Generation, plotted for allowed terms from section 4.2.2

maximum absorption coefficient is 52000 cm^{-1} , and drops quickly as the wavelength increases, or energy decreases. This maximum absorption coefficient is equivalent to direct gap absorption coefficient. Even though the absorption coefficient is high at higher energies, thermalization of the photo-generated will counter the effect. In case of absorption coefficient for quantum dots, the absorption coefficient is not only high, but also more spread over the wavelength, to give an improved spectrum for absorption of photons.

Chapter 5

COMPARISON OF ABSORPTION COEFFICIENT WITH SOLAR CELL EFFICIENCY

This chapter will relate the calculated absorption coefficient with the solar cell efficiency.

The model used here is that of a $p^+ - i - n^+$ junction solar cell. The structure of the solar cell, and associated physics equations have been discussed in this chapter as we go along.

5.1 The Solar Cell Structure Design

The model used for the solar cell structure is a generic $p^+ - i - n^+$ junction cell shown in figure 5.1. It consists of alternating stacked layers of QDs in the intrinsic region, to enhance the photo-generated current. The effective band gap for absorption in each many-QD layer is determined by the lowest confined states of the QDs. The approach is basically to produce structures with engineered band gap. For the same purpose, silicon nanocrystals embedded in the silicon dielectric matrix can be used [1, 32]. As shown in section B.1, the quantum confined energy levels increase the effective band gap of the nanostructure as compared to bulk silicon. The energy band diagram for the structure is shown in figure 5.2.

Dr. Conibeer and his group have fabricated such structures using silicon [1], and other materials such as GaAs/InAs have been also fabricated in such a fashion [33]. For our work, we are considering silicon nanostructures confined in all three dimensions i.e. QDs, embedded in SiO_2 matrix. These multi-stacked layers can be deposited by sputtering alternating "stoichiometric dielectric / Si-rich dielectric" process, followed by annealing. At the annealing temperature, the Si in the Si-rich dielectric precipitates out, and crystallizes between the stoichiometric layers [1]. The size of the QD can be controlled by the thickness of the Si-rich layer between the stoichiometric layers. Dopant layers can be co-sputtered while sputtering Si-rich layer, if the doping of dots is required. Due to strong coupling between QDs, electronic states demonstrate wire-like character [34], due to which the electrons and the holes are channeled through. This serves as an efficient mechanism for separating the

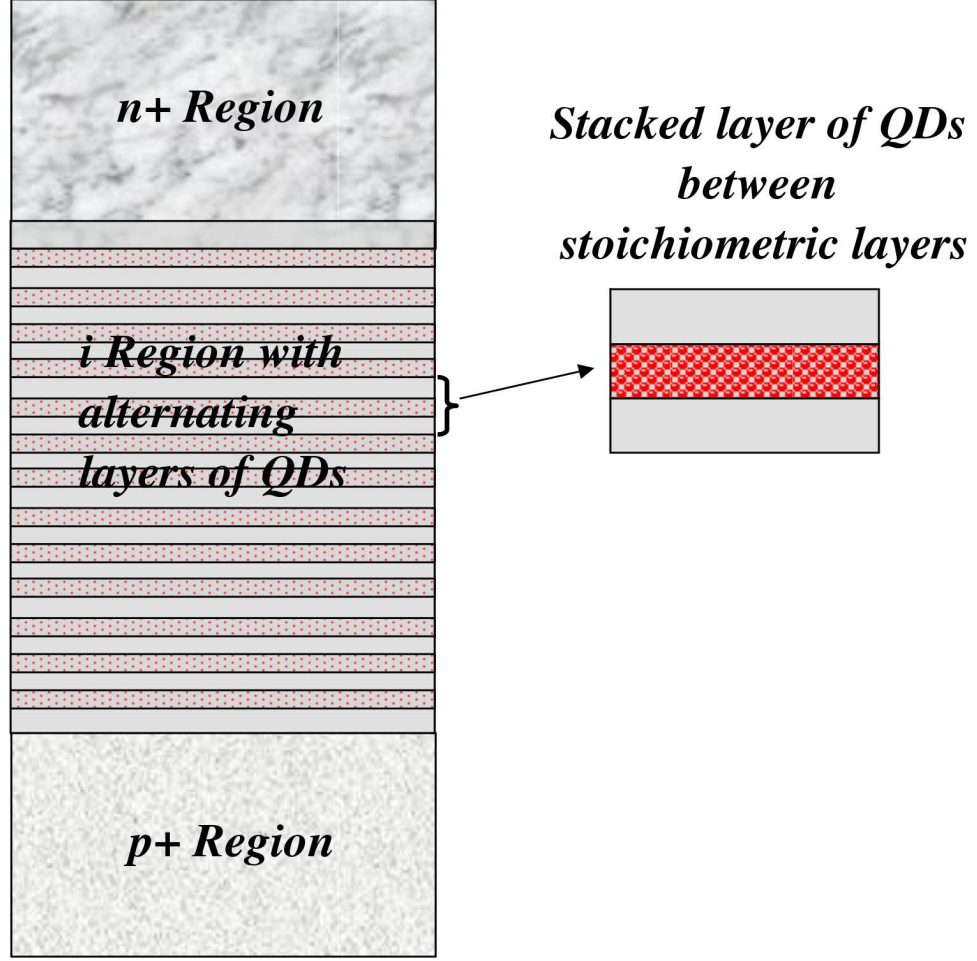


Figure 5.1: Schematic of a $p^+ - i - n^+$ designed solar cell structure

generated electrons and holes in QDs across the p and n regions.

5.2 Photocurrent in the Solar Cell

We can calculate the photocurrent by the solving the minority carrier transport equation in each of the possible regions. For convenience purposes, this thesis will only compare

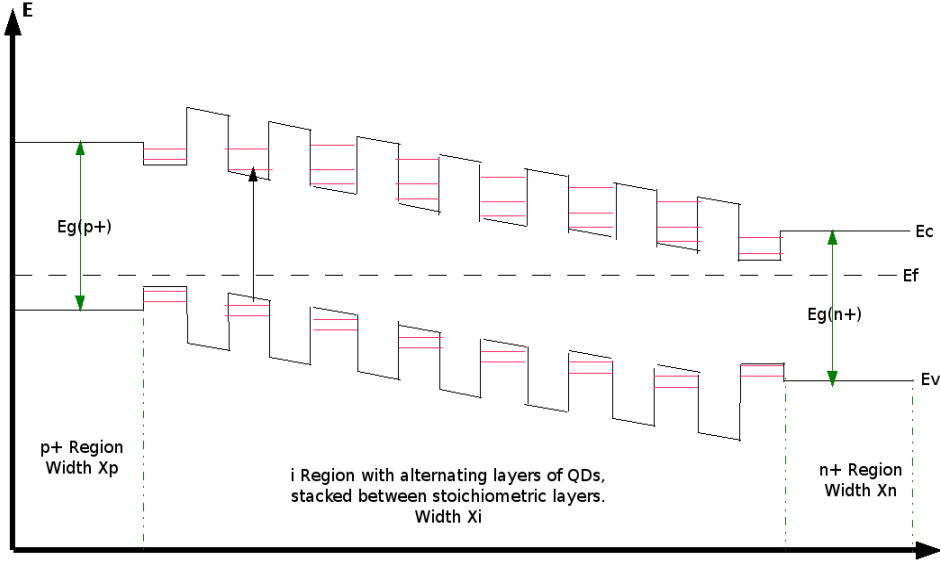


Figure 5.2: Energy band diagram of the $p^+ - i - n^+$ solar cell shown in figure 5.1

the currents in the intrinsic region, and study the contribution of QDs to the generated photocurrent in the i -region.

Carrier confinement exhibited by the QDs, quantizes the energy spectrum into discrete levels. This is shown in figure 5.2. The absorption edges in these QDs are shifted to higher energies due to this confinement effect. The photo-carrier generation rate G_{QD} for the QDs can be written as

$$G_{QD}(\lambda, X) = \Phi(\lambda) [1 - R(\lambda)] \alpha_{QD}(\lambda) \exp(-\alpha_{QD}(X - X_n)) \quad (5.1)$$

$\Phi(\lambda)$ is the spectral distribution of solar flux incident on solar cell, $R(\lambda)$ is the reflection

coefficient for the surface of the solar cell, and X is the distance of the QDs from the surface of the cell. The assumption here is that the top surface, or the surface exposed to light or solar flux is the n^+ region of width X_n . If the top surface is the p^+ region, then the term $(X - X_n)$ changes to $(X - X_p)$. α_{QD} is the absorption coefficient for quantum dots. The total photocurrent from the QDs can then be written as

$$j_{QD}(\lambda) = e \int_{X_n}^{X_n + X_i} G_{QD}(\lambda, X) dx \quad (5.2)$$

For the stoichiometric layers, they will also generate some current. The fraction occupied by this region will be $(1 - QD_{vol})$. If n_{QD} is the volume density for the QDs, and V_{QD} is the average volume for one QD, then the fraction occupied by stoichiometric layers is $(1 - n_{QD} V_{QD})$. The generation rate for this region is

$$G_S(\lambda, X) = \Phi(\lambda) [1 - R(\lambda)] \exp(-\alpha(\lambda) X_n) (1 - n_{QD} V_{QD}) \alpha_S(\lambda) \exp(-(1 - n_{QD} V_{QD}) \alpha_S (X - X_n)) \quad (5.3)$$

The photo-generated current due to this generation can be written as

$$j_S(\lambda) = e \int_{X_n}^{X_n + X_i} G_S(\lambda, X) dx \quad (5.4)$$

The total current over the whole solar spectrum can now be written as

$$J_i = e \left(\int_{\lambda_{min}}^{\lambda_{max}} (j_s + j_{QD}) d\lambda \right) \quad (5.5)$$

Using the above calculated current equations in the intrinsic region, and the equations for efficiency calculations shown in section A.1, we can calculate the currents, and efficiencies for varying parameters. The above equations are under certain assumptions such as the diffusion length of carriers is assumed larger than the width of the intrinsic region (X_i), so that most of the generated carriers in the region are swept out by the junction field without any recombination losses. Thus as the width of the intrinsic region increases, recombination losses governed by the impurity levels increases. There exists a limit to the maximum number of QD layers we can have in the intrinsic region. Hence there exists an optimum number of QD layers due to competition between the light absorption and recombination losses [33].

5.3 Practical Efficiency Calculations

We will use the following values for the various parameters in the calculation of short circuit current in the intrinsic region. The solar flux is assumed to be equivalent to black body radiation at a temperature of 5760k, given as using Plank's Law,

$$\Phi(\lambda) = \frac{2\pi\hbar c^2}{\lambda^5} \left\{ \exp\left(\frac{2\pi\hbar c}{kT\lambda}\right) - 1 \right\} \quad (5.6)$$

We use the reflection coefficient as 0.1. The values for absorption coefficient is used from those derived in chapter 3, and calculated in chapter 4. For the silicon QDs, we assume that minimum band gap attained for confined quantum dots is 1.29 eV , and the maximum band gap is 3.65 eV . The other parameters assumed are as shown in table 5.1.

PARAMETERS	VALUE	UNITS
Maximum Band Gap for Silicon QD (for 1.8nm QD)	3.65	eV
Maximum Band Gap for Silicon QD (for 7nm QD)	1.29	eV
Length of i-region (X_i)	3	μm
Surface Reflection Coefficient ($R(\lambda)$)	0.1	-
Volume of QD (V_{QD})	1.77×10^{-18}	cm^3
Volume Density of QDs (n_{QD})	1.7×10^{17}	cm^{-3}
Band Gap of Stoichiometric Material assumed as Silicon	1.12	eV

Table 5.1: Parameter Values for short circuit current in intrinsic region

We calculate the current using the above parameters. The intrinsic region devoid of QDs is assumed to be silicon with a band gap of 1.12 eV . For calculation purposes, the band gap is assumed direct gap. On using the above values, the ratio of current for intrinsic region with QDs to current in intrinsic region without QDs ($n_{QD} = 0$) (i.e. intrinsic region is made of undoped silicon of direct band gap 1.12 eV), comes out to be 1.865. Hence, keeping other factors constant, we can improve the efficiency by a factor of 1.865 times. Thus for a solar cell of efficiency of 26% for first generation solar cell, we can improve the efficiency to

nearly 48.5% on using QDs.

Chapter 6

CONCLUSION AND FUTURE WORK

This work has made an attempt to plot the absorption coefficient vs. wavelength in nanostructure silicon using quantum mechanical based calculations. The absorption coefficient shows a peak of 64638.2 cm^{-1} at $\lambda = 343 \text{ nm}$ at photon energy of $\xi = 3.49 \text{ eV}$ ($\lambda = 355.532 \text{ nm}$). I have shown that a large value of absorption coefficient α comparable to that of bulk silicon is possible in silicon QDs because of carrier confinement. This carrier confinement leads to direct band to band transition resulting in a very large value of oscillator strength in the calculation of transition probabilities. A comparison of PL including excitonic effects in nanostructure silicon further confirms our estimated theoretical plots, knowing that optical absorption and PL are closely related.

The concept of solar cell is described in brief in chapter5. Using the absorption coefficient

calculated in chapter 4, we have shown that the efficiency of a p-i-n junction solar cell can be significantly increased through the use of stacked QD layers in the intrinsic region. The QDs increases the short circuit current. There is not much effect on the open circuit voltage by the QDs.

One of the optical parameters used in our calculations is refractive index. A lot of work should be devoted for detailed calculation of refractive index vs. wavelength plot in nanostructure silicon. A better understanding of oscillator strength in nanostructure is required for understanding the quantum confinement in better details.

It is very important to relate solar cell efficiency to the optical absorption. A very generic approach has been used in calculation of efficiency for a solar cell. There are a lot of assumptions taken, which will not be true in reality. We will further investigate the dependence of efficiency not only on optical absorption but also on photon capture and reflection based on fundamental principles. Hence the overall efficiency calculation for a QD based solar cell requires a detailed treatment of electronic band structure, carrier emission, capture, recombination mechanisms and other current losses in the cell.

Appendix A

MATHEMATICAL PROOFS

A.1 Shockley-Queisser Limit

The principle of detailed balance limit [5], for calculation of limiting efficiency in a single p-n junction device, has been used in this work. The current-voltage relationship for a solar cell may be written as

$$I_{net} = I_{sc} + I_0 \left(1 - \exp \frac{V_{net}}{V_{sol}} \right) \quad (\text{A.1})$$

$$= I_0 \left(\exp \frac{V_{op}}{V_{sol}} - \exp \frac{V_{net}}{V_{sol}} \right) \quad (\text{A.2})$$

Here I_{net} and V_{net} are the net current and voltage generated. I_0 is the reverse saturation current for the p-n junction. V_{oc} is the open circuit voltage and I_{sc} is the short circuit current. V_{sol} is the solar cell bias. For maximum power ($P = I_{net}V_{net}$), $\frac{dP}{dV_{net}} = 0$, which using equation A.2, can be written as

$$I_0 \left(\exp \frac{V_{op}}{V_{sol}} - \left(\frac{V_{net} + V_{sol}}{V_{sol}} \right) \exp \frac{V_{net}}{V_{sol}} \right) = 0 \quad (A.3)$$

Let the solution to above equation A.3 be V_{max} . The current for this solution, I_{max} , can be calculated using equation A.2. The fill factor (FF), or the squareness of the I-V curve for solar cell, can then be calculated as

$$FF = \frac{V_{max} I_{max}}{V_{oc} I_{sc}} \quad (A.4)$$

The fill factor FF is sometimes also referred to as the *impedance matching factor*, m. Solving for FF, using equation A.2 and A.3, we get

$$FF = \frac{\left(\frac{V_{max}}{V_{sol}} \right)^2}{\left(1 + \frac{V_{max}}{V_{sol}} - \exp - \frac{V_{max}}{V_{sol}} \right)} \left(\frac{V_{max}}{V_{sol}} + \ln \left(1 + \frac{V_{max}}{V_{sol}} \right) \right) \quad (A.5)$$

For defining the efficiency of the solar cell, we can use above equation A.5, in the equation

for efficiency. The efficiency is defined as

$$\eta = \frac{V_{max} I_{max}}{P_{input}} = \frac{V_{oc} I_{sc} FF}{P_{input}} \quad (\text{A.6})$$

The principle of detailed balance limit uses the assumption, that the probability of photon with energy greater than band gap to produce an electron-hole pair is unity. Using the parameters as defined by Shockley-Queisser [5], for a single junction made of Silicon with bandgap of 1.12 eV, the efficiency limit comes out to be 31%. With infinite junctions made of silicon, the limit comes out to be 68%.

Appendix B

PHYSICAL PROOFS

B.1 Quantum Confinement in Silicon Quantum Dot Structures

The effective mass solution, or the EMA of the Schrödinger equation for electrons confined in three dimension for a quantum dot is same as that for the EMA of a one dimension confinement in case of quantum well. For a quantum dot of size (or diameter 'a'), if we consider a very large confining potential, we can write,

$$\vec{k}a = n\pi \tag{B.1}$$

k is the wavevector. For n 'th confined energy level, the increase in energy is given by

$$\Delta E_n = \frac{\hbar^2 k^2}{2m^*} \quad (\text{B.2})$$

Using B.1 in B.2, the discrete levels of confined energy in one of the dimensions are

$$\Delta E_n = \frac{\hbar^2 \pi^2}{m^* a^2} n^2$$

If we consider confinement in all three directions, the above equation can be written for n_1 , n_2 , n_3 as

$$\Delta E_n = \frac{\hbar^2 \pi^2}{m^* a^2} (n_1^2 + n_2^2 + n_3^2) \quad (\text{B.3})$$

For a quantum dot, $n_1 = n_2 = n_3 = n$, and thus the confined energy levels are

$$\Delta E_n = \frac{\hbar^2 \pi^2}{m^* a^2} 3n^2 \quad (\text{B.4})$$

The above equation B.5 is very similar to that obtained for two dimensional quantum well confined in one dimension. There is just an added factor of 3, which shows that quantum

dots have confined energy levels three times those of quantum wells. The corresponding energy levels for the quantum well in quantum dot are those which are non-degenerate with the same quantum number. If we consider a cubic quantum dot, we can say that for a given confined state, a quantum dot has a diameter $\sqrt{3}$ times the width of the corresponding quantum well. It has been experimentally observed that for a spherical quantum dot, the diameter for a given confined state is nearly 2 times the width of the corresponding quantum well [35].

For calculation purposes, we use the conduction effective masses of $m_e^* = 0.27 m_0$, and $m_h^* = 0.59 m_0$ (considering contributions of both light hole and heavy hole). Using these values for B.5, we can write the first quantized ground energy state as

$$E_1 = E_g + \Delta E_1$$

For spherical quantum dots, the value of ΔE_1 obtained for cubic quantum dots, should be divided by $\left(\frac{\sqrt{3}}{2}\right)^2$ to account for the increased confinement. Hence, on solving, we get (plotted in figure B.1)

$$E_1 = E_g + \frac{609}{\left(\frac{\sqrt{3}}{2}\right)^2 a^2} \quad (\text{B.5})$$

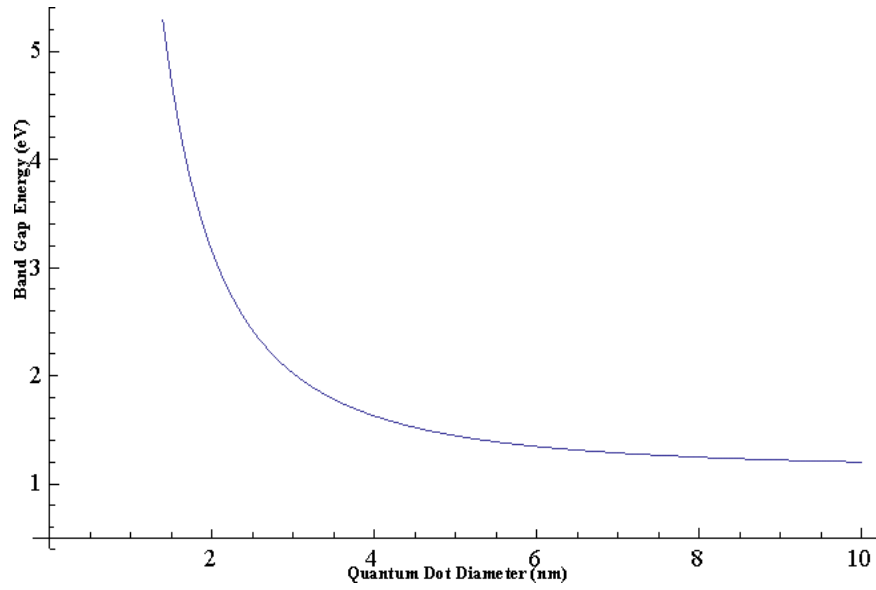


Figure B.1: Band Gap for Silicon Quantum Dots' calculated by EMA Approximation

The bandgap for 10 *nm* dot is nearly 1.2012 eV, and for 1.8 *nm* dot it is 3.65 eV.

Appendix C

PERMISSION FOR IMAGE REPRINT

C.1 Chapter 1: 1

1.1: Solar Tree - This image is free.

1.2: Solar Spectrum - Permitted under Academic and Non-commercial Use.

1.3: PV World Production - This file has been (or is hereby) released into the public domain by its author, Geoffrey Landis at the wikipedia project. This applies worldwide. Author grants anyone the right to use this work for any purpose, without any conditions, unless such conditions are required by law.

1.4: Solar Cell Efficiency - This image is a work of a United States Department of Energy (or predecessor organization) employee, taken or made during the course of an employee's official duties. As a work of the U.S. federal government, the image is in the public domain.

1.5, 1.6, 1.8:

Permission to use images in my thesis

Gavin Conibeer <g.conibeer@unsw.edu.au> Thu, Nov 18, 2010 at 3:55 AM

To: Jaspreet Singh <jnayyar@mtu.edu>

Dear Jaspreet

Yes this should be OK.

But please ensure to give due acknowledgement.

Regards

Gavin

From: jaspreetsn@gmail.com [mailto:jaspreetsn@gmail.com] On Behalf Of Jaspreet Singh

Sent: Thursday, 18 November 2010 2:14 PM To: Gavin Conibeer Subject: Permission to use images in my thesis

Hi Gavin

I wanted to use the following images in my thesis for Masters in Electrical Engineering.

1. LOSS PROCESSES IN A STANDARD SOLAR CELL - from the Annual Report 2005, Section 4.5, figure 4.5.1
2. ALL SILICON TANDEM SOLAR CELL - from the Annual Report 2009, Section 4.5.2.1, figure 4.5.2
3. EFFICIENCY AND COST PROJECTIONS - from Annual Report 2004 Section 4.5, figure 4.8

I would be obliged if you can grant me the permission to use these images in my thesis, and reprint them.

Regards – Jaspreet S Nayyar

Grad Student - ECE, MSE

Michigan Tech

www.linkedin.com/in/jaspreetnayyar

References

- [1] Conibeer, G. *Nanoscale Photonics and Cell Technologies for Photovoltaics II* 7411.
- [2] Pagliaro, M.; Palmisano, G.; Ciriminna, R. *Flexible Solar Cells*; Wiley, John & Sons, Incorporated: Weinheim, 2008.
- [3] Ciamician, G. *Science* **1912**, 36, 385.
- [4] Nelson, J. *The Physics of Solar Cells*; 2003.
- [5] Shockley, W.; Queisser, H. J. *Journal of Applied Physics* **1961**, 32, 510.
- [6] Green, M. A. *Third Generation Photovoltaics: Advanced Solar Energy Conversion*; Springer Berlin: Heidelberg, 2006.
- [7] Mathew, X.; Enriquez, J. P.; Tiwari, A.; Romeo, A. *Solar Energy* **2004**, 77, 831.
- [8] Johnson, D. C.; Ballard, I. M.; Barnham, K. W.; Connolly, J. P.; Mazzer, M.; Bessière, A.; Calder, C.; Hill, G.; Roberts, J. S. *Applied Physics Letters* **2007**, 90, 213505.
- [9] Green, M. A.; Keevers, M. *Progress in Photovoltaics* 3, 189.

- [10] Cudra, L.; Marti, A.; Luque, A. *Physica E* **14**, 162.
- [11] Luque, A.; Marti, A. *Electronic Letters* **2008**, *44*, 943.
- [12] Wolfe, C. M.; Holonyak, N.; Stillman, G. E. *Physical Properties of Semiconductors*; Prentice Hall: New Jersey, 1989.
- [13] Nayyar, J. S.; Kulkarni, A. K. *Nanoscale Photonic and Cell Technologies for Photovoltaics II, SPIE 7411*.
- [14] Schiff, L. I. *Quantum Mechanics*; McGraw Hill: New York, 1955.
- [15] Delley, B.; Steigmeier, E. F. *Physical Review B* **47**.
- [16] Smith, R. A. *Wave Mechanics of Crystalline Solids*; Wiley, 1961.
- [17] van Roosbroeck, W.; Shockley, W. *Physical Review* **1954**, *94*, 1558.
- [18] Muth, J. F.; Lee, J. H.; Shmagin, I. K.; Kolbas, R. M.; Jr, H. C. C.; Seller, B. P.; Mishra, U. K.; DenBaars, S. P. *Applied Physics Letters* **1997**, *71*, 2572.
- [19] Wang, L.-W.; Zunger, A. *Physical Review Letters* **73**, 1039.
- [20] Tripathy, S.; Soni, R. K.; Ghoshal, S. K.; Jain, K. P. *Bulletin of Material Science* **24**, 258.
- [21] Iakoubovskii, K.; Mitsuishi, K.; Nakayama, Y.; Furuya, K. *Physical Review B* **2008**, *77*, 104102.

- [22] Zaknoon, B.; Bahir, G.; Saguy, C.; Edrei, R.; Hoffman, A.; Rao, R. A.; Muralidhar, R.; Chang, K. *Nano Letters* **8**, 1689.
- [23] Holmes, J. D.; Zeigler, K.; Doty, R. C.; Pell, L. E.; Johnston, K. P.; Korgel, B. A. *J. Amer. Chem. Soc.* **123**, 3743.
- [24] Warner, J. H.; Hoshino, A.; Yamamoto, K.; Tilley, R. D. *Angewandte Chemie International Edition* **44**, 4550.
- [25] Poruba, A.; Fejfar, A.; Remeš, Z.; Špringer, J.; Vaněček, M.; Kočka, J.; Meier, J.; Torres, P.; Shah, A. *Journal of Applied Physics* **2000**, *88*, 148.
- [26] Bass, M. *Handbook of Optics, 2nd ed.*; McGraw Hill: New York, 1995.
- [27] Smith, A.; Yamani, Z. H.; Roberts, N.; Turner, J.; Habbal, S. R.; Granick, S.; Nayfeh, M. H. *Physical Review B* **2000**, *72*, 205307.
- [28] Schmitt-Rink, S.; Miller, D. A.; Chemla, D. S. *Physical Review B* **1987**, *35*, 15.
- [29] Parm, I. O.; Yi, J. *Material Sc. and Engg. B.* **134**, 130.
- [30] Allan, G.; Delerue, C.; Lannoo, M. *Journal of Luminescence* **57**, 239.
- [31] Kanemitsu, Y.; Nakaoshi, Y.; Masumoto, Y. *Phys. Rev. B* **1992**, *46*, 3916.
- [32] Honsberg, C. B.; Barnett, A. M.; Kirkpatrick, D. *Photovoltaic Energy Conversion, IEEE 4th World Conference* **2006**, *2*, 2565.

- [33] amd S. Petrosyan, V. A.; Khachatryan, A.; Touryan, K. *Journal of Applied Physics* **2001**, 89, 2268.
- [34] Darhuber, A. A.; Holy, V.; Stangl, J.; Bauer, G.; Krost, A.; Heinrichsdorff, F.; Grundmann, M.; Bimberg, D.; Ustinov, V. M.; Kop'ev, P. S.; Kosogov, A. O.; Werner, P. *Applied Physics Letter* **1997**, 70, 955.
- [35] Ribeiro, F. J.; Latg, A. *Phys. Rev. B* **1994**, 50, 4913.

Index

- Absorption Coefficient, 41
 - Bulk Solar Cell, 67
- Direct Gap
 - Allowed Term, 42
 - Forbidden Term, 43
- Excitonic Transition, 47
- Indirect Band Gap
 - Conduction Band Virtual State, 45
 - Forbidden Transition, 46
 - Valence Band Virtual State, 45
- Bloch's Theorem, 36
- Dirac-Delta Function, 30
- DOS, 21, 48
 - Fermi Energy Dependence, 48, 57
- Effective Mass, 57
 - Electron, 57
 - Hole, 57
- Electron Transition Probability, 21, 29, 30, 39, 41
- EMA, 83
- Exciton, 46
 - Binding Energies, 46, 63
- Maxwell Equations, 23
- Oscillator Strength, 40, 57
 - Direct Gap
 - Allowed Term, 40
 - Forbidden Term, 42
 - Indirect Band Gap
 - For Conduction Band, 45
 - For Valence Band, 45
- Permissions, 87
 - Chapter 1, 87
- Photoluminescence, 51, 64
- Photon Absorption, 33

Exciton Transition, 46, 63	Si, 83
Intra-Band Absorption, 34, 56	Refractive Index, 54
Allowed Transition Probability, 39	Herzberger's Formula, 55
Direct Gap, 34, 57, 59	Si, 55
In-Direct Gap, 43, 62	
Photon vector mag, 23	Shockley-Queisser Limit, 19
Photon-Electron Interaction, 22	Shockley-Queisser Limit, 11, 79
First Order Perturbation Theory, 27	Detailed Balance Limit, 79
Interaction Hamiltonian, 24	Solar Cells
Perturbed Hamiltonian for Interaction, 24	Bulk or Thick Film, <i>see</i> First Generation
Schrödinger equation	Solar Cells
Time Dependent, 24	Current Generation, <i>see</i> Third Generation
Time Independent, 25	tion Solar Cells
Transition Matrix Element, 26	Efficiency, 81
Unperturbed Hamiltonian, 24	Fill Factor, 80
Poynting Vector, 41	Generations of Solar Cells, 6
	First Generation, 7
Quantum Confinement, 14, 21	Second Generation, 8
Effective Mass Solution, <i>see</i> EMA	Third Generation, 10
QDs	History, 4
Cubical, 85	Hot Carrier Solar Cell, 17
Spherical, 85	I-V Relationship, 79

Loss Mechanisms, 14

Nanostructured Solar Cells, 11

p-i-n Structure, 70

Photocurrent, 71

Tandem Solar Cell, 16

Thin Film, *see* Second Generation Solar
Cells

Up-Down Conversion Solar Cell, 17

Solar Spectrum, 1

Vector Potential, 22